iScience

CellPress
OPEN ACCESS

Article

ACSL1 is a key regulator of inflammatory and macrophage foaming induced by short-term palmitate exposure or acute high-fat feeding

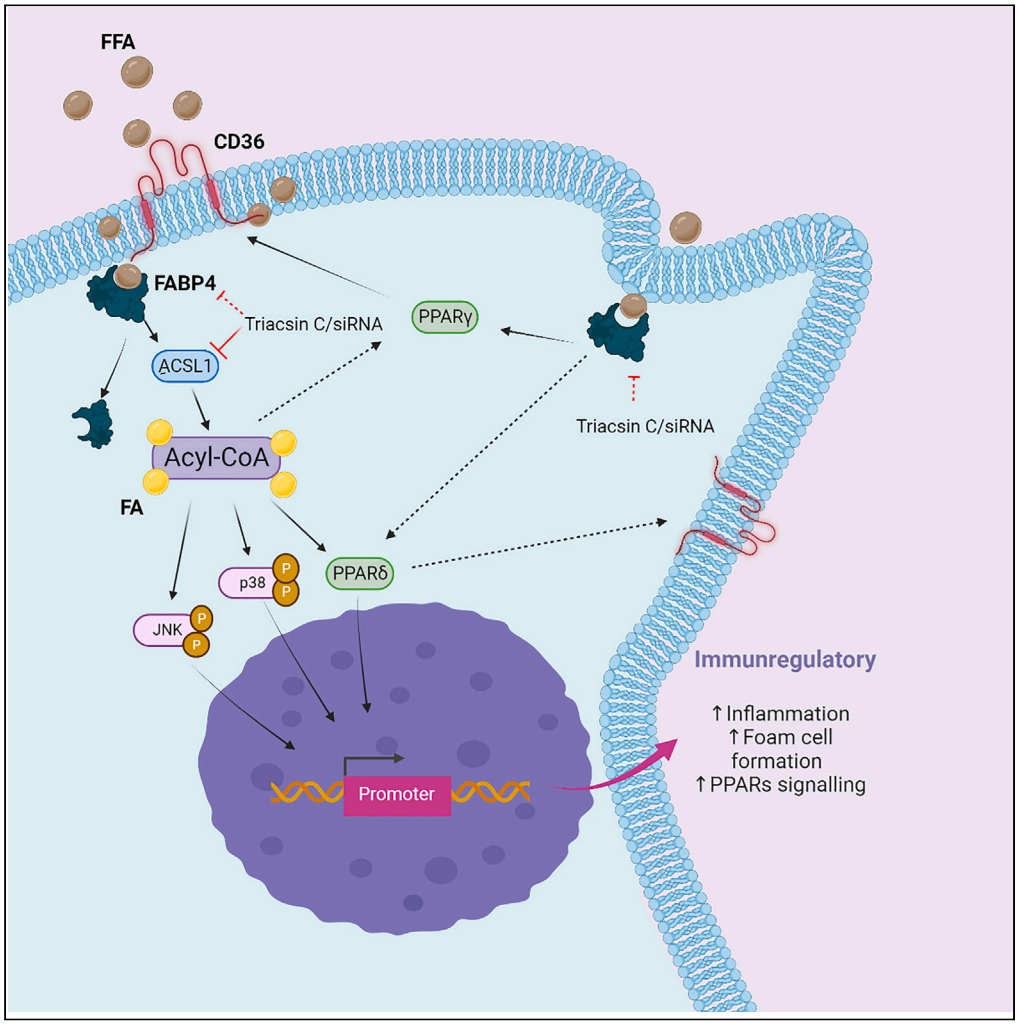

Fatema Al-Rashed, Dania Haddad, Ashraf Al Madhoun, ..., Fahd Al-Mulla, Yusuf A. Hannun, Rasheed Ahmad

rasheed.ahmad@dasmaninstitute.org

Highlights

Short-term palmitate exposure induces ACSL1

ACSL1 activates the CD36/p38/PPARδ axis to induce macrophage foaming and inflammation

ACSL1 is necessary for PPARs-induced CD36 activation involving FABP4

ACSL1 inhibition suppresses AHFF-induced inflammatory and foamy monocytes in mice

Al-Rashed et al., iScience *26*, 107145
July 21, 2023
https://doi.org/10.1016/j.isci.2023.107145

iScience

CellPress
OPEN ACCESS

Article

ACSL1 is a key regulator of inflammatory and macrophage foaming induced by short-term palmitate exposure or acute high-fat feeding

Fatema Al-Rashed,[1] Dania Haddad,[2,5] Ashraf Al Madhoun,[2,3,5] Sardar Sindhu,[1,3] Texy Jacob,[1] Shihab Kochumon,[1] Lina M. Obeid,[4] Fahd Al-Mulla,[2] Yusuf A. Hannun,[4] and Rasheed Ahmad[1,6,*]

SUMMARY

Foamy and inflammatory macrophages play pathogenic roles in metabolic disorders. However, the mechanisms that promote foamy and inflammatory macrophage phenotypes under acute-high-fat feeding (AHFF) remain elusive. Herein, we investigated the role of acyl-CoA synthetase-1 (ACSL1) in favoring the foamy/inflammatory phenotype of monocytes/macrophages upon short-term exposure to palmitate or AHFF. Palmitate exposure induced a foamy/inflammatory phenotype in macrophages which was associated with increased ACSL1 expression. Inhibition/knockdown of ACSL1 in macrophages suppressed the foamy/inflammatory phenotype through the inhibition of the CD36-FABP4-p38-PPARδ signaling axis. ACSL1 inhibition/knockdown suppressed macrophage foaming/inflammation after palmitate stimulation by downregulating the FABP4 expression. Similar results were obtained using primary human monocytes. As expected, oral administration of ACSL1 inhibitor triacsin-C in mice before AHFF normalized the inflammatory/foamy phenotype of the circulatory monocytes by suppressing FABP4 expression. Our results reveal that targeting ACSL1 leads to the attenuation of the CD36-FABP4-p38-PPARδ signaling axis, providing a therapeutic strategy to prevent the AHFF-induced macrophage foaming and inflammation.

INTRODUCTION

Malfunctioning lipid metabolism marks the pathogenesis of obesity and obesity-related complications such as diabetes, hepatic steatosis, atherosclerosis, and cardiovascular disease.[1–3] Macrophage-derived foam cells with proinflammatory phenotype play a key role in the pathophysiology of atherosclerosis.[4] Increasing evidence supports that a single high-fat meal or acute high-fat feeding (AHFF) may temporarily raise serum triglycerides, causing the formation of triglyceride-rich lipoproteins (TRL) and inflammation.[5–7] Henning et al. showed that the consumption of a high-fat meal increased the potential of monocytes to become foam cells and develop an inflammatory phenotype.[8] As the first step in foam cell formation following high-fat feeding, naive circulatory monocytes are recruited to the subendothelial spaces where they mature into residential, potentially lipid-laden macrophages that play a key role in metabolic inflammation.[9] Macrophages engulf modified LDL and circulating free fatty acids (FFAs), such as palmitate (PA), by endocytosis or through cell surface scavenger receptor CD36[10–12] and are transformed into foam cells with an inflammatory phenotype. However, the mechanisms that promote foamy and inflammatory macrophage phenotype following a short-term PA exposure or AHFF remain elusive.

Conversion of FFAs into acyl-CoAs is required for the initiation of lipid metabolism.[13] The addition of a coenzyme-A (CoA) group to a fatty acid to form fatty acyl-CoA is catalyzed by the long-chain fatty acyl-CoA synthetase or ligase (ACSL) family of enzymes, effectively "trapping" fatty acids intracellularly. Fatty acyl-CoAs serve as substrates in lipid and protein metabolism and are responsible for channeling fatty acids to produce glycerolipids, sphingolipids, and for beta-oxidation in mitochondria.[14,15]

We and others previously showed that overexpression of ACSL family members enhances the fatty acid uptake in metabolic syndrome, leading to changes in cellular physiology and inflammatory status.[16,17]

[1]Immunology & Microbiology Department, Dasman Diabetes Institute, Kuwait City, Dasman 15462, Kuwait

[2]Genetics and Bioinformatics Department, Dasman Diabetes Institute, Kuwait City, Dasman 15462, Kuwait

[3]Animal and Imaging Core Facilities, Dasman Diabetes Institute, Kuwait City, Dasman 15462, Kuwait

[4]Stony Brook Cancer Center, Stony Brook University, Stony Brook, NY 11794, USA

[5]These authors contributed equally

[6]Lead contact

*Correspondence: rasheed.ahmad@dasmaninstitute.org

https://doi.org/10.1016/j.isci.2023.107145

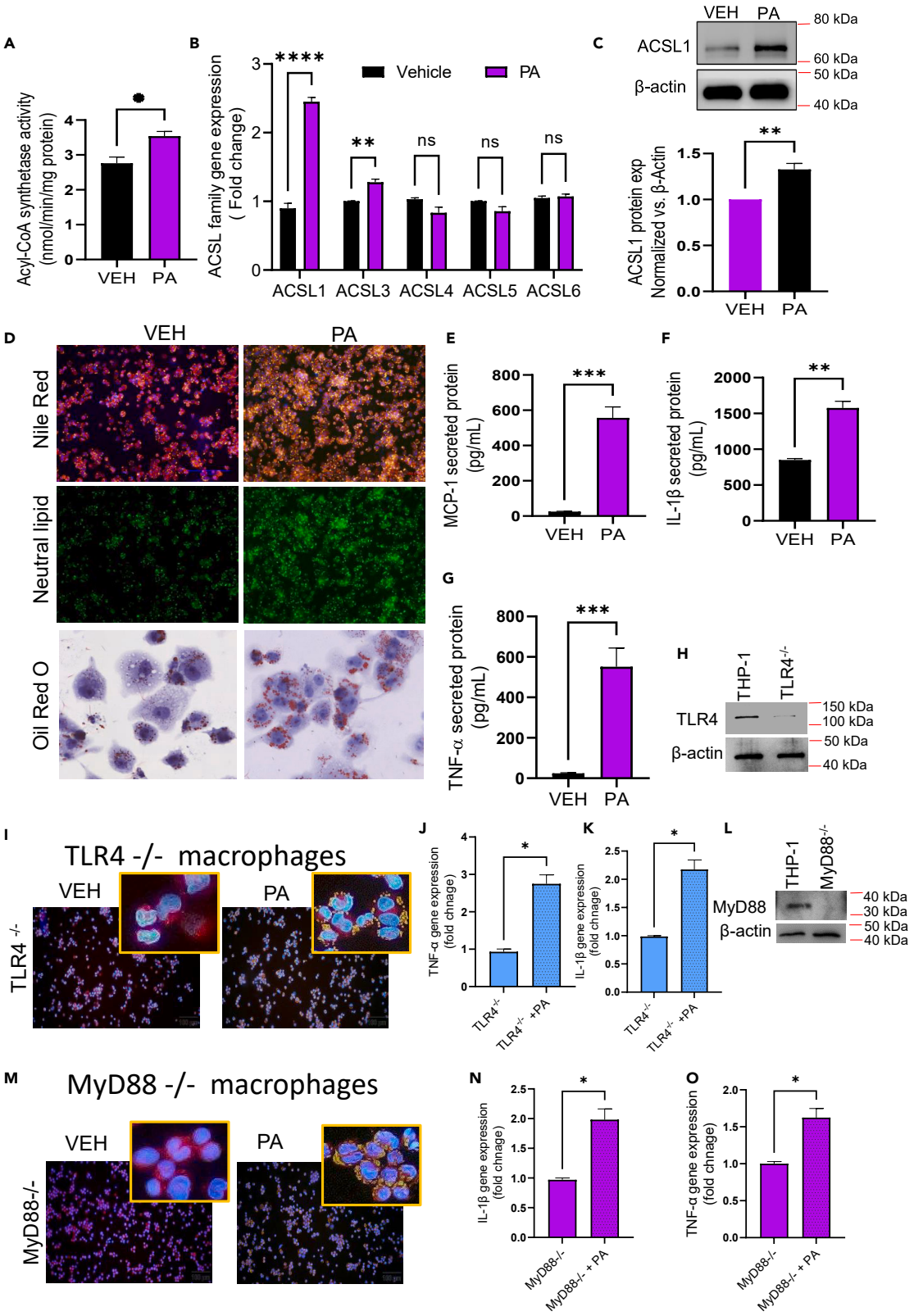
A
Acyl-CoA synthetase activity (nmol/min/mg protein)
VEH
PA
B
ACSL family gene expression (Fold change)
Vehicle
PA
****
**
ns
ns
ns
ACSL1
ACSL3
ACSL4
ACSL5
ACSL6
C
VEH
PA
ACSL1
β-actin
80 kDa
60 kDa
50 kDa
40 kDa
ACSL1 protein exp Normalized vs. β-Actin
**
D
VEH
PA
Nile Red
Neutral lipid
Oil Red O
E
MCP-1 secreted protein (pg/mL)
***
F
IL-1β secreted protein (pg/mL)
**
G
TNF-α secreted protein (pg/mL)
***
H
THP-1
TLR4-/-
TLR4
β-actin
150 kDa
100 kDa
50 kDa
40 kDa
I
TLR4 -/- macrophages
VEH
PA
TLR4 -/-
J
TNF-α gene expression (fold chnage)
TLR4-/-
TLR4-/- +PA
K
IL-1β gene expression (fold chnage)
L
THP-1
MyD88-/-
MyD88
β-actin
40 kDa
30 kDa
50 kDa
40 kDa
M
MyD88 -/- macrophages
VEH
PA
MyD88-/-
N
IL-1β gene expression (fold chnage)
MyD88-/-
MyD88-/- + PA
O
TNF-α gene expression (fold chnage)
MyD88-/-
MyD88-/- + PA

Figure 1. Short-term palmitate stimulation increases ACSL1 expression and promotes foam cell formation and inflammation in macrophages

THP-1-derived macrophages were treated with 150μM of palmitate (PA) for 4 h and controls were treated with vehicle (0.1% BSA) only. Cells were harvested for total RNA or total protein extraction as described in STAR Methods.

(A) Short-term PA stimulation enhances the ACSL enzymatic activity in an equal amount of protein (50μg) ($p < 0.05$).

(B) Gene expression of ACSL isoforms was determined using qRT-PCR.

(C) Representative Western blot showing significant induction of ACSL1 protein expression in macrophages. 3-4 replicates were used for western blot quantification.

(D) Representative images (Scale bar 50 μm) of Nile Red immunofluorescence and Oil Red O staining depicting lipid accumulation in macrophages (foam cell formation) following short-term PA stimulation compared to control treated with vehicle only.

(E–G) Analysis of secreted inflammatory mediators by ELISA reveals significant induction of MCP-1, IL-1β, and TNF-α in conditioned media from macrophages treated with PA for 24 h compared to vehicle-treated controls.

(H) Western blot of the lysates from wild type and TLR4−/− macrophages.

(I) Representative images (Scale bar 100 μm) of Nile Red Staining of TLR4−/− macrophages after treatment with vehicle and PA.

(J and K) TNF-α and IL-1β expression in TLR4−/− macrophages.

(L) Western blot of the lysates from wild type and MyD88−/− macrophages.

(M) Representative images (Scale bar 100 μm) of Nile Red Staining of MyD88−/− macrophages after treatment with vehicle and PA.

(N and O) TNF-α and IL-1β expression in MyD88−/− macrophages Data are presented as mean ± SEM values (n = 3-4) and compared between groups using unpaired t-test. *$p \leq 0.05$, **$p \leq 0.01$, ***$p \leq 0.001$, ****$p \leq 0.0001$.

However, it remains unclear whether ACSL1 regulates foaming and inflammation in macrophages, following their short-term exposure to a saturated free fatty acid such as palmitate, a condition essentially mimicking the *in vivo* effect of AHFF. We, therefore, determined the role of ACSL1 in the regulation of inflammatory and macrophage foaming induced by short-term palmitate exposure or acute high-fat feeding and investigated the signal transduction pathway(s) involved.

RESULTS

Palmitate upregulates ACSL1 expression and promotes foam cell formation and inflammation in macrophages

To determine whether the ACSL expression was modulated in response to short-term exposure to palmitate, THP-1-derived macrophages were treated with PA for 4 h and total ACSL enzymatic activity was assessed. ACSL enzymatic activity was found to be significantly upregulated ($p < 0.05$) in macrophages following short-term PA treatment (Figure 1A), suggesting the functional relevance of the ACSL. To further dissect the effect of PA short-term treatment on the expression of the ACSL family members, we assessed gene expression of ACSL1, ACSL3, ACSL4, ACSL5, and ACSL6 and found that PA short-term treatment significantly increased the expression of both ACSL1 and ACSL3 in macrophages, while the reduction in ACSL4 and ACSL5 mRNA expression did not reach statistical significance. No change in ACSL6 mRNA expression was observed following short-term PA treatment of macrophages (Figure 1B). Notably, based on the most remarkable gene induction of ACSL1 compared to ACSL3 in macrophages following short-term PA stimulation (Figure 1B), and reported wider subcellular distribution[18] and highest expression in immune cells,[19] we next focused on the ACSL1 isoenzyme and further confirmed its increased protein expression in macrophages following short-term PA exposure (Figure 1C).

Given that short-term PA stimulation enhance the ACSL1 transcripts and protein expression in macrophages, we asked whether the upregulated ACSL1 activity/expression led to an increased lipid uptake causing foam cell formation and expression of proinflammatory chemokines/cytokines. As expected, macrophages subjected to short-term PA treatment displayed increased lipid content and foam cell formation as demonstrated by Nile Red immunofluorescence or Oil Red O staining (Figure 1D). Additionally, we determined the role of another plausible ligand such as OxLDL regarding macrophage foaming and inflammation and the data show that similar to pamitate, OxLDL also induces macrophage foaming and inflammation (Figures S1A–S1D). These foam cells also actively produced proinflammatory mediators including MCP-1, IL-1β, and TNF-α when challenged with short-term PA treatment (Figures 1E–1G).

Palmitate can serve as the agonists of the innate immune receptor toll like receptor 4 (TLR4). Therefore, we questioned whether our observed effects of palmitate on macrophages require TLR4. Our data show that TLR4−/− macrophages give a similar response to palmitate for foaming and inflammation (IL-1β, TNF-α), suggesting that palmitate-induced macrophage foaming (Nile Red) and inflammation is independent of TLR4 (Figures 1H–1K). TLR4 mediates signaling through Myeloid differentiation primary response 88 (MyD88)-dependent pathways to activate an inflammatory response, we also used MyD88−/− macrophages to further clarify the

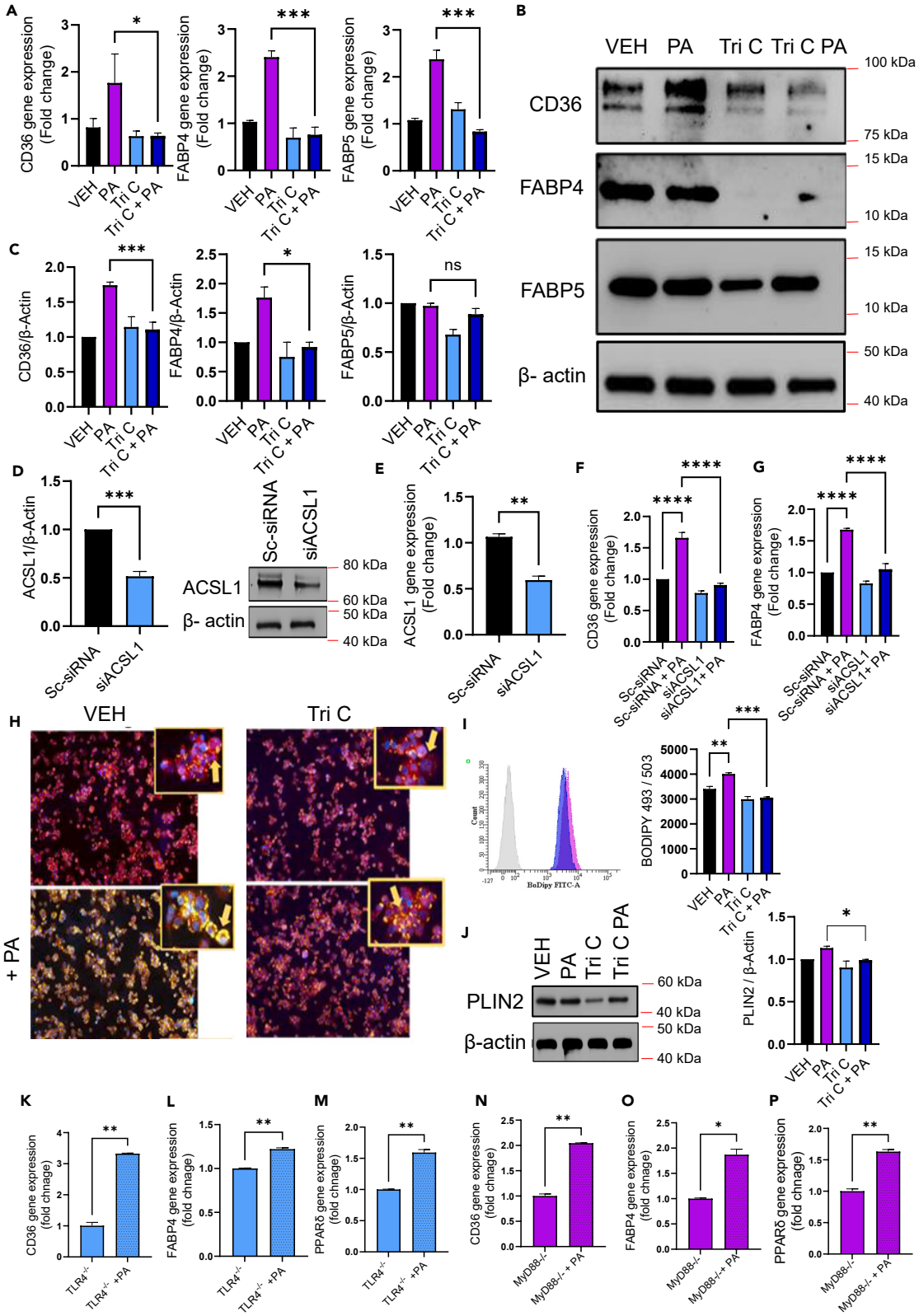
A
CD36 gene expression (Fold change)
FABP4 gene expression (Fold change)
FABP5 gene expression (Fold change)
VEH
PA
Tri C
Tri C + PA
B
VEH PA Tri C Tri C PA
CD36
FABP4
FABP5
β- actin
100 kDa
75 kDa
15 kDa
10 kDa
15 kDa
10 kDa
50 kDa
40 kDa
C
CD36/β-Actin
FABP4/β-Actin
FABP5/β-Actin
ns
D
ACSL1/β-Actin
Sc-siRNA
siACSL1
ACSL1
β- actin
80 kDa
60 kDa
50 kDa
40 kDa
E
ACSL1 gene expression (Fold change)
F
CD36 gene expression (Fold change)
Sc-siRNA + PA
siACSL1 + PA
G
FABP4 gene expression (Fold change)
H
VEH
Tri C
+ PA
I
BODIPY 493 / 503
BoDipy FITC-A
J
PLIN2
β-actin
60 kDa
40 kDa
50 kDa
40 kDa
PLIN2 / β-Actin
K
CD36 gene expression (fold chnage)
TLR4-/-
TLR4-/- +PA
L
FABP4 gene expression (fold chnage)
M
PPARδ gene expression (fold chnage)
N
CD36 gene expression (fold chnage)
MyD88-/-
MyD88-/- + PA
O
FABP4 gene expression (fold chnage)
P
PPARδ gene expression (fold chnage)

Figure 2. ACSL1 inhibition or deficiency leads to a marked defect in the expression of CD36 and FABP4 in macrophages subjected to short-term palmitate stimulation

THP1-derived macrophages were stimulated with -palmitate (PA; 150μM) for 4 h and controls were treated with vehicle (0.1% BSA) only. For pharmacological inhibition of ACSL1, macrophages were treated with ACSL1 inhibitor triacsin C (5 μM; T4540), followed by stimulation with PA (150 μM) for 4 h. For ACSL1 genetic silencing, macrophages were transfected with 20 nM, each, of gene-specific and control (scrambled) siRNAs using Viromer Blue (Lipocalyx, Halle, Germany), following the manufacturer's instructions and later, cells were stimulated with PA (150 μM) for 4 h. Cells were harvested for total RNA or total protein extraction as described in STAR Methods.

(A) Analysis of lipid uptake genes CD36, FABP4, and FABP5 was made by qRT-PCR.

(B) Representative immunoblots showing significant protein suppression of CD36 and FABP4 in macrophages that were pre-treated with triacsin C; however, no suppression of FABP5 protein was detected. Three replicates were used for western blot quantification.

(C) Immunoblots quantification data shown for protein expression of CD36, FABP4, and FABP5.

(D) Representative immunoblots and quantification data indicating significant protein suppression of ACSL1 in macrophages transfected with ACSL1-siRNA.

(E–G) Gene expression (qRT-PCR) analysis revealing significant downregulation of ACSL1, CD36, and FABP4 transcripts in cells transfected with ACSL1-siRNA compared to sc-siRNA transfected controls.

(H) Representative images (Scale bar 50μM) of Nile Red immunofluorescence staining showing reduced lipid accumulation in triacsin C-treated macrophages following short-term PA stimulation compared to controls stimulated with palmitate only.

(I) Flow cytometry (BODIPY 493/503 stating) analysis indicating significantly reduced lipid accumulation in triacsin C-treated macrophages stimulated with PA compared to controls stimulated with PA only.

(J) Representative immunoblots showing significantly reduced perilipin (PLIN)-2 protein expression in triacsin C-treated macrophages following short-term PA stimulation compared to controls treated with PA only.

(K–M) TLR4 −/− macrophages were treated with PA. CD36, FABP4, and PPARδ gene expression was determined.

(N–P) MyD88−/− macrophages were treated with PA. CD36, FABP4, and PPARδ gene expression was determined. Data were presented as mean ± SEM (n = 3-8) and compared between two groups using unpaired t-test and between more than two groups using one-way ANOVA with Tukey's test. *$p \leq 0.05$, **$p \leq 0.01$, ***$p \leq 0.001$, ****$p \leq 0.0001$.

role of TLR4 in this palmitate-induced foaming (Nile Red staining) and inflammation (IL-1β, TNF-α). Our data show that MyD88−/− macrophages showed foaming and inflammation in response to palmitate (Figures 1L–1O) which further ruled out the involvement of TLR4. Collectively, these data support a model in which short-term PA treatment of macrophages upregulates the ACSL1 isoenzyme activity and expression and promotes foam cell formation and inflammation in macrophages.

Pharmacologic inhibition or genetic suppression of ACSL1 leads to a marked defect in lipid uptake and foam cell formation via reduced expression of CD36, FABP4, and PLIN2

Since we found that ACSL1 expression was consistent with a foamy and inflammatory phenotype of macrophages, we next asked whether ACSL1 expression affects the expression of genes involved in fatty acids (FA) transport and processing. To this end, macrophages were pretreated with triacsin C, an inhibitor of ACSLs, before short-term PA treatment. Pharmacologic inhibition of ACSL1 led to a significant decrease in transcripts expression of FA uptake and transport regulator genes including the lipid scavenger receptor CD36 ($p < 0.05$) and fatty acid binding proteins (FABP)-4 & 5 ($p < 0.01$) (Figure 2A). Additionally, we found that the pharmacologic inhibition of ACSL1 suppressed OxLDL-induced CD36 and FABP4 expression in macrophages (Figures S1E and S1F). As expected, a significant reduction in protein expression of CD36 ($p < 0.0001$) and FABP4 ($p < 0.05$) was also observed as detected by western blotting. No significant change was seen in FABP5 (Figures 2B and 2C). Whereas ACSL1 inhibition did not affect the expression of fatty acid oxidation genes including CPT1A and CPT2 (Figure S2A) and on *de novo* fatty acid synthesis gene ACACA (Figure S2B). To further confirm the role of ACSL1, we transfected macrophages with ACSL1 siRNA and achieved about a 50% reduction in ACSL1 protein and mRNA levels as compared to scrambled siRNA (Figures 2D and 2E, respectively). As with pharmacologic inhibition using triacsin C treatment, genetic suppression by ACSL1 siRNA also reduced ($p < 0.0001$) the gene expression of CD36 (Figure 2F) and FABP4 (Figure 2G) but not FABP5 (Figure S2C) following short-term PA treatment compared to scrambled siRNA-transfected cells.

Given that FA uptake and transport proteins were upregulated in macrophages after short-term PA treatment, we next sought to measure the cellular lipid content in short-term PA-stimulated macrophages following ACSL1 inhibition by triacsin C. To this effect, as expected, Nile Red staining and BODIPY 493/503 flowcytometric analysis showed a dramatic decrease in neutral lipid accumulation following a short-term PA stimulation of triacsin C-treated cells ($p < 0.001$) (Figures 2H and 2I). We also found that ACSL1 inhibition by triacsin C significantly reduced the protein expression of lipid-droplet associated Perilipin 2 (PLIN2) ($p < 0.001$), indicating that ACSL1 is essential for both lipid uptake/transport and lipid-droplet formation (Figure 2J). To validate the effect of ACSL1 inhibition on FA uptake, we conducted a

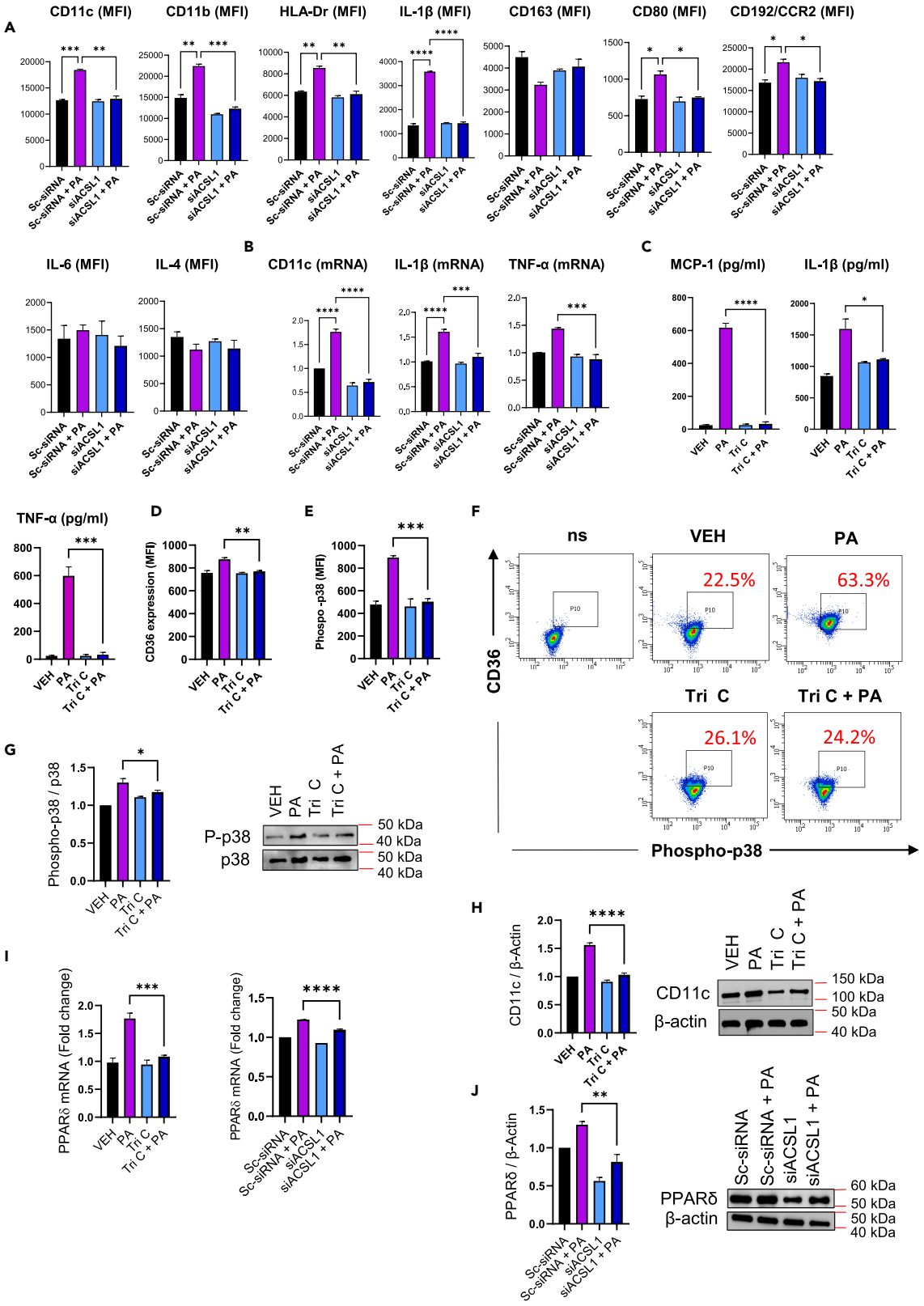
A
CD11c (MFI)
CD11b (MFI)
HLA-Dr (MFI)
IL-1β (MFI)
CD163 (MFI)
CD80 (MFI)
CD192/CCR2 (MFI)
Sc-siRNA
Sc-siRNA + PA
siACSL1
siACSL1 + PA
B
IL-6 (MFI)
IL-4 (MFI)
CD11c (mRNA)
IL-1β (mRNA)
TNF-α (mRNA)
C
MCP-1 (pg/ml)
IL-1β (pg/ml)
TNF-α (pg/ml)
D
CD36 expression (MFI)
E
Phospo -p38 (MFI)
VEH
PA
Tri C
Tri C + PA
F
ns
VEH
PA
22.5%
63.3%
Tri C
Tri C + PA
26.1%
24.2%
CD36
Phospho-p38
G
Phospho-p38 / p38
P-p38
p38
50 kDa
40 kDa
50 kDa
40 kDa
H
CD11c / β-Actin
CD11c
β-actin
150 kDa
100 kDa
50 kDa
40 kDa
I
PPARδ mRNA (Fold change)
PPARδ mRNA (Fold change)
J
PPARδ / β-Actin
PPARδ
β-actin
60 kDa
50 kDa
50 kDa
40 kDa

Figure 3. ACSL1 knockdown or inhibition prevents inflammatory phenotype expression in short-term palmitate-stimulated macrophages via CD36/p38/PPAR mediated pathways

THP1-derived macrophages were stimulated with palmitic acid (PA; 150μM) for 4 h and controls were treated with vehicle (0.1% BSA) only. For ACSL1 genetic silencing, macrophages were transfected with 20 nM, each, of gene-specific and control (scrambled) siRNAs using Viromer Blue (Lipocalyx, Halle, Germany), following the manufacturer's instructions and later, cells were stimulated with PA (150 μM) for 4 h. Cells were harvested for total RNA or total protein extraction as described in STAR Methods.

(A) Flow cytometry analysis of macrophage inflammatory markers expression including CD11c, CD11b, HLA-DR, IL-1β, CD163, CD80, CD192, IL-6, and IL-4 shown as mean fluorescence intensity (MFI) in ACSL1 deficient cells. Flow cytometry analysis of macrophage markers reveals significant suppression of inflammatory proteins including CD11c, CD11b, HLA-DR, IL-1β, CD80, CD192/CCR2, and IL-6 in triacsin C-treated macrophages following short-term PA stimulation, compared to controls treated with PA only; while, no significant suppression was observed regarding pan-macrophage marker CD163 and anti-inflammatory cytokine marker IL-4.

(B) qRT-PCR analysis of macrophage inflammatory markers CD11c, IL-1β, and TNF-α in macrophages deficient in ACSL1.

(C) ELISAs for secreted inflammatory mediators display significantly reduced production of MCP-1, IL-1β, and TNF-α in culture supernatants of triacsin C-treated macrophages following short-term PA stimulation, compared to controls treated with PA only.

(D and E) Flow cytometry data (MFI) graphs show highly diminished expression of CD36 scavenger receptor and phospho p38 MAPK proteins in triacsin C-treated macrophages following short-term PA stimulation, compared to controls treated with PA only.

(F) Representative dot-plots displaying the reduced CD36+phospho p38+ co-expression in triacsin C-treated macrophages following short-term PA stimulation, compared to controls treated with PA only.

(G) Representative immunoblots showing significant reduction of p38 MAPK phosphorylated protein expression in triacsin C-treated macrophages following short-term PA stimulation, compared to controls treated with PA only.

(H) Representative immunoblots depicting significantly less CD11c protein expression in triacsin C-treated macrophages following short-term PA stimulation, compared to controls treated with PA only.

(I) Gene expression (qRT-PCR) analysis shows significantly downregulated expression of PPARδ in triacsin C-treated macrophages following short-term PA stimulation, compared to controls treated with PA only, as well as in ACSL1 siRNA-transfected macrophages subjected to short-term PA stimulation, compared to sc-siRNA-transfected controls following short-term PA stimulation.

(J) Representative immunoblots showing significantly reduced PPARδ protein expression in ACSL1 siRNA-transfected macrophages, compared to sc-siRNA-transfected controls, following short-term PA stimulation. 3-4 replicates were used for western blot quantification. Data are presented as mean ± SEM values (n = 3), and were analyzed using one-way ANOVA with Tukey's test. ns:non-significant, *p ≤ 0.05, **p ≤ 0.01, ***p ≤ 0.001, ****p ≤ 0.0001.

time-dependent assay by treating macrophages with ACSL1 inhibitor triacsin C either before, during, or after PA stimulation. Nile Red staining indicated that ACSL1 inhibition was significantly effective when triacsin C was administered 30-60 min before short-term PA stimulation. However, the effect was relatively less significant when triacsin C was co-administered with PA, while no significant effect was induced when triacsin C was administered an hour after PA stimulation (Figures S2D and S2E). Since palmitate can serve as an agonist of the innate immune receptor TLR4. Therefore, we determined whether our observed effects of palmitate on macrophages require TLR4. Our data show that TLR4−/− macrophages give a similar response to palmitate for CD36 and FABP4, suggesting that palmitate-induced CD36 and FABP4 is independent of TLR4 (Figures 2K–2M). TLR4 mediates signaling through MyD88-dependent pathways to activate an inflammatory response, we also used MyD88−/− macrophages to further clarify the role of TLR4 in this palmitate-induced CD36 and FABP4. Our data show that MyD88−/− macrophages showed expression of CD36 and FABP4 in response to palmitate (Figures 2N–2P).Overall, these data support that following short-term PA stimulation, ACSL1 regulates the expression of CD36, FABP4, and PLIN2, leading to intracellular lipid accumulation and foam cell formation in macrophages.

Pharmacologic inhibition of ACSL1 or genetic suppression prevents the short-term PA treatment-induced inflammatory phenotype in macrophages via the CD36/p38/PPARδ signaling axis

The ingestion of a single high-fat meal was shown to induce acute postprandial inflammatory and metabolic responses within 6 h of ingestion in healthy individuals.[20–22] Also, the involvement of ACSL1 in several monocytic/macrophage inflammatory responses has been shown previously by our group and others.[16,23] However, the role played by this lipid metabolism enzyme in inflammatory macrophage responses to short-term PA stimulation remains unclear. Our data show that short-term PA stimulation upregulates the expression of macrophage infiltration and inflammatory markers including CD11c, CD11b, HLA-DR, CD163, CD80, CD192/CCR2, IL-6, IL-1β, and TNF-α at the transcriptional and/or translational levels. However, PA-induced expression of these markers was significantly reduced ($P<0.05$) in siRNA transfected ACSL1 knockdown macrophages compared to those transfected with control siRNA (Figures 3A and 3B) Similarly, the expression of inflammatory markers was significantly decreased in the cells that were pretreated with triacsin C before short-term PA treatment (Figures S3A and S3B). Furthermore, ACSL1 inhibition by triacsin C abolished the secretion of pro-inflammatory mediators including MCP-1, IL-1β, and TNF-α in response to short-term PA treatment (Figure 3C).

The role of CD36 in immunity, metabolism, and atherogenesis is well recognized. Scavenger receptor CD36 mediates FFA uptake, leading to the upregulation of inflammatory responses involving p38 and JNK pathways.[12,24–26] To understand how ACSL1 inhibition modulates inflammatory signaling, changes in the expression of CD36 and CD11b were assessed in triacsin C-treated macrophages following short-term PA stimulation. ACSL1 inhibition by triacsin C suppressed short-term PA stimulation-induced upregulation of CD36 ($p < 0.01$) (Figure 3D) and CD11b surface markers ($p < 0.01$) (Figure 3A). Furthermore, triacsin C-treated macrophages showed ~60% reduction in phospho p38 expression after short-term PA stimulation compared to controls ($p < 0.001$) (Figures 3E and 3F), while ~50% downregulation in JNK phosphorylation was observed (Figures S4B and S4C). To further verify the role of ACSL1 inhibition in p38 signaling, expression of p38 phosphorylation was analyzed by western blotting, and a significant suppression ($p < 0.05$) of p38 phosphorylation was documented in triacsin C-treated $CD11b^{+}CD36^{+}$ macrophages following short-term PA stimulation compared to control (Figure 3G). In parallel, we also observed suppression of inflammatory marker CD11c in triacsin C-treated cells (Figure 3H). Taken together, these data suggest that ACSL1 inhibition curbs the short-term PA stimulation-induced inflammatory responses downstream of CD36 by suppressing p38-and JNK-mediated signaling.

PPARs are involved in the transcriptional control of glucose and energy metabolism. These are also key players in mitochondrial physiology, cholesterol metabolism, and inflammatory responses in macrophages.[27] PPARs are also involved in FFA-induced cellular changes and were reported to mediate oxidized LDL-induced CD36 expression.[28] To investigate if PPARs family members were involved in short-term PA stimulation-induced inflammatory responses in $CD11b^{+}CD36^{+}$ macrophages, we measured the expression of the PPARα, PPARδ, and PPARγ in PA-stimulated macrophages in which ACSL1 activity was impaired by triacsin C-treatment or ACSL1 siRNA transfection. To this end, we found that short-term PA treatment induced a significant gene upregulation of PPARδ which was significantly downregulated following triacsin C treatment ($p < 0.001$) or siRNA-mediated ACSL1 genetic suppression ($p < 0.0001$), compared to respective controls (Figures 3I and S1G). As expected, ACSL1 gene silencing also paralleled with reduced PPARδ protein expression ($p < 0.01$) in response to short-term PA stimulation compared to controls (Figure 3J).

Interestingly, short-term PA treatment induced a significant reduction of the PPARα gene expression in macrophages, which was partially restored by short-term PA stimulation in macrophages that were treated with triacsin C or transfected with ACSL1 siRNA, albeit non-significantly. However, no significant changes in PPARγ gene expression were observed in short-term PA stimulated macrophages, with or without ACSL1 inhibition or genetic suppression (Figure S4E). Overall, these data support the role of ACSL1 as a key player in short-term PA stimulation-induced inflammatory responses downstream of the CD36 scavenger receptor through signaling mechanisms that involve p38 and PPARδ pathways.

PPARs-induced CD36 activation leading to macrophage foaming is dependent on ACSL1-associated FABP4 expression

The interactions between PPARs and CD36 were previously found to be bidirectional, with PPARγ shown to induce CD36 expression.[29] However, it is still unclear if PPARδ has a similar inductive effect on CD36 expression. To understand this dynamic, CD36 gene expression was investigated in response to PPARδ and PPARγ agonists including GW0742 and rosiglitazone, respectively. Both agonists upregulated the CD36 gene expression (Figure 4A) and promoted the ACSL activity (Figure 4B).

Based on these findings, to further understand the dynamics of how ACSL1 silencing impacts the CD36 and PPARδ expression, lipid accumulation, and inflammation, Western blot analysis indicated that PPARδ protein expression was reversibly suppressed by ACSL1 deficiency as the treatment of ACSL1 siRNA-transfected cells with GW0742 significantly ($p < 0.0001$) restored protein expression of PPARδ back to expression levels in controls. Nonetheless, the impaired PPARδ protein expression in ACSL1-deficient cells could not be fully rescued by treatment of ACSL1 siRNA-transfected cells with rosiglitazone, compared to scrambled siRNA-transfected controls (Figures 4C and 4F). Further analysis regarding CD36 protein expression showed that PPARδ agonist GW0742 was able to rescue CD36 expression in ACSL1-deficient cells, whereas PPARγ agonist rosiglitazone did not, compared to their respective controls (Figures 4D and 4F). Notably, FABP4 protein expression was reduced in ACSL1-deficient cells and did not change significantly after stimulation with both PPARs agonists (Figures 4E and 4F). This observation suggests the possibility of a direct relationship between ACSL1 and FABP4 expression in macrophages, independent of PPARs γ and δ. To test this, double immunofluorescence staining for both ACSL1 and FABP4 was conducted to assess the

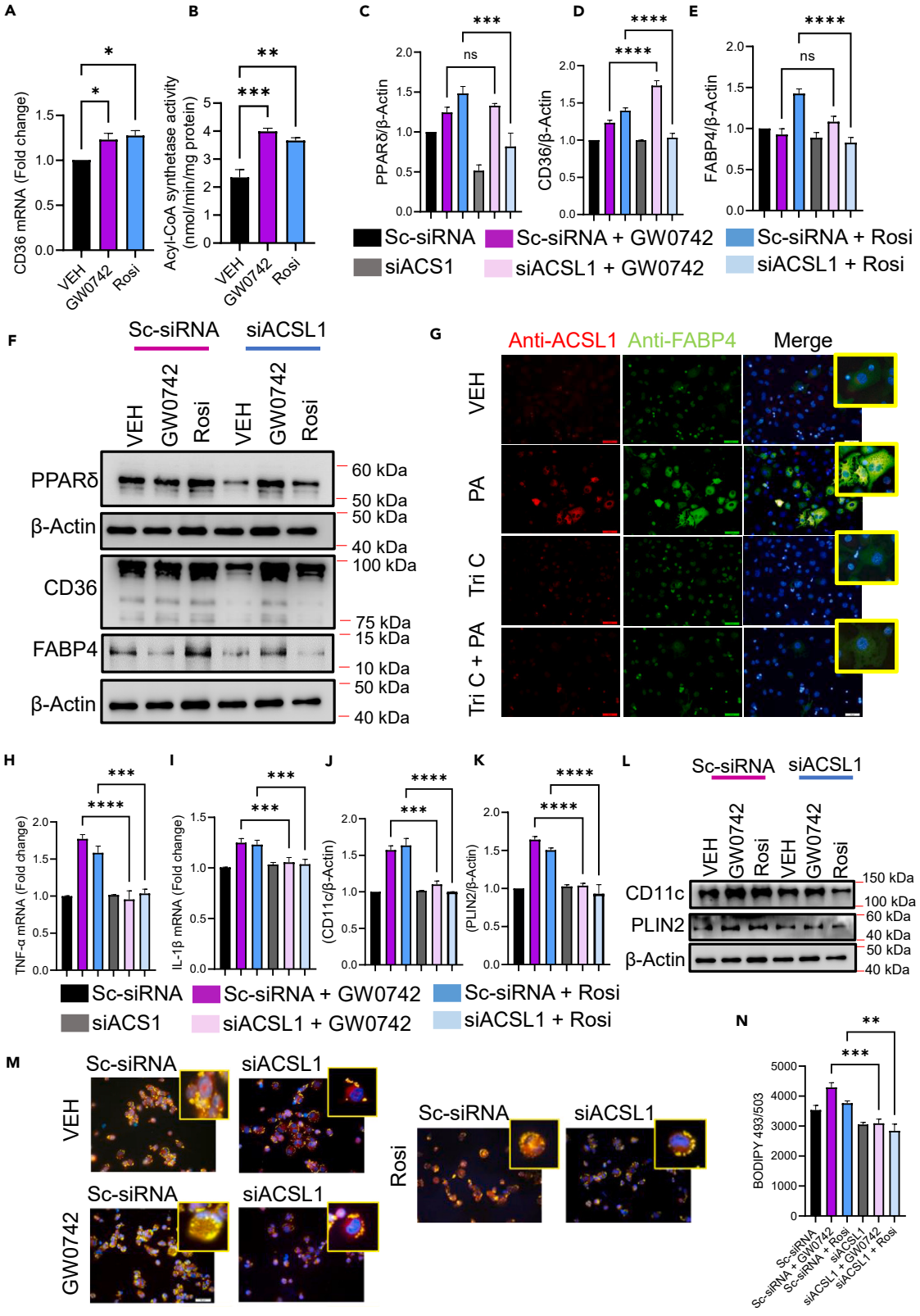
A
CD36 mRNA (Fold change)
VEH
GW0742
Rosi
B
Acyl-CoA synthetase activity (nmol/min/mg protein)
C
PPARδ/β-Actin
D
CD36/β-Actin
E
FABP4/β-Actin
ns
Sc-siRNA
Sc-siRNA + GW0742
Sc-siRNA + Rosi
siACS1
siACSL1 + GW0742
siACSL1 + Rosi
F
Sc-siRNA
siACSL1
PPARδ
β-Actin
CD36
FABP4
60 kDa
50 kDa
40 kDa
100 kDa
75 kDa
15 kDa
10 kDa
G
Anti-ACSL1
Anti-FABP4
Merge
VEH
PA
Tri C
Tri C + PA
H
TNF-α mRNA (Fold change)
I
IL-1β mRNA (Fold change)
J
(CD11c/β-Actin)
K
(PLIN2/β-Actin)
L
CD11c
PLIN2
150 kDa
100 kDa
60 kDa
M
N
BODIPY 493/503

Figure 4. PPARs-induced CD36 activation associated with macrophage foaming involves ACSL1-dependent FABP4 expression

For stimulation studies, THP1-derived macrophages were pre-treated with PPARδ agonist GW0742 (1μM), PPARγ agonist rosiglitazone (1μM), and ACSL1 inhibitor triacsin C (5 μM; T4540) for 30-60 min and then stimulated with PA (150 μM) for 4 h at 37°C and controls were treated with vehicle (0.1% BSA) only. For ACSL1 genetic silencing studies, transformed macrophages were transfected with 20 nM, each, of gene-specific and control (scrambled) siRNAs using Viromer Blue (Lipocalyx, Halle, Germany), following the manufacturer's instructions and then cells were stimulated with PA (150 μM) for 4 h. Cells were harvested for total RNA or total protein extraction as described in STAR Methods.

(A) Gene expression (RT-PCR) analysis shows a significant upregulation of CD36 transcripts following macrophage stimulation with agonists of PPARδ (GW0742) and PPARγ (rosiglitazone).

(B) ACSL enzymatic activity in an equal amount of protein (50μg) is significantly enhanced in macrophages following treatments with agonists of PPARs γ and δ.

(C-F) Analysis of the immunoblots and representative immunoblots showing PPARδ, CD36, and FABP4 proteins in macrophages following treatments with PPAR-γ/δ agonists.

(G) Representative confocal microscopy images demonstrate the co-localization of ACSL1 and FABP4 proteins in transformed macrophages induced by short-term PA stimulation, while the PA-induced FABP4 expression is reduced in triacsin C-treated ACSL1-defective macrophages.

(H and I) Gene expression (qRT-PCR) analysis of macrophage inflammatory markers displays the increased induction of TNF-α and IL-1β transcripts in macrophages following stimulation with agonists of PPARs -δ (GW0742) and -γ (rosiglitazone); however, this PPARs agonism failed to rescue gene expression of these inflammatory mediators in ACSL1-deficient macrophages.

(J and L) Representative immunoblots show induction of CD11c and PLIN2 proteins in macrophages stimulated with GW0742 (PPAR-δ agonist) and rosiglitazone (PPAR-γ agonist), while the stimulation by these PPAR agonists failed to rescue expression of these proteins in ACSL1-deficient macrophages.

(M) Representative images (Scale bar: 50μM) of Nile Red immunofluorescence depicting induction of intracellular lipid accumulation in macrophages after stimulation with PPAR-δ agonist GW0742 and PPAR-γ agonist rosiglitazone while this PPARs agonism did not rescue lipid accumulation in ACSL1-deficient macrophages.

(N) Flow cytometry (BODIPY 493/503 staining) analysis corroborating microscopy data by showing induction of intracellular lipids in macrophages following PPARs stimulation by GW0742 (PPAR-δ agonist) and rosiglitazone (PPAR-γ agonist), whereas PPARs agonism failed to rescue intracellular lipid accumulation in ACSL1-deficient macrophages. 3-4 replicates were used for western blot quantification. Data were presented as mean ± SEM (n = 3) and were compared by using one-way ANOVA with Tukey's test. ns: non-significant, *$p \leq 0.05$, **$p \leq 0.01$, ***$p \leq 0.001$, ****$p \leq 0.0001$.

co-expression of the ACSL1 and FABP4. The confocal microscopy images show that short-term PA stimulation leads to the co-localization of ACSL1 (in red) and FABP4 (in green) expression in macrophages which is decreased significantly following short-term PA stimulation of the triacsin C-treated (ACSL1-deficient) macrophages (Figure 4G).

We next wanted to see whether the ACSL1 deficiency led to a stable or irreversible suppression of inflammatory phenotypic markers in macrophages. To this effect, the data show that PPAR-γ/-δ agonism in ACSL1-defective macrophages failed to rescue the inflammatory phenotype with consistently lower expression of TNF-α, IL-1β, and CD11c as compared to respective controls (Figures 4H–4J).

ACSL1 and PLIN2 are known to interact with lipid droplets.[30,31] We further sought to know if the PPARs (γ/δ) agonism could rescue the PLIN2 suppression in ACSL1-deficient macrophages. To this end, we found that reduced PLIN2 expression in ACSL1 siRNA-transfected macrophages could not be restored following treatments with GW0742 or with rosiglitazone, compared to controls (Figures 4K and 4L), indicating that macrophages with defective ACSL1 activity are less likely to accumulate lipids and transform into inflammatory foam cells, despite the GW0742-induced CD36 activation. To see how lipid accumulation was modulated in response to short-term PA stimulation, both ACSL1 siRNA-transfected and scrambled siRNA-transfected macrophages were treated with agonists of PPARδ (GW0742) or PPARγ (rosiglitazone) to activate CD36 expression, followed by short-term PA stimulation. Lipid accumulation was assessed by Nile Red immunofluorescent staining and by flow cytometry using BODIPY staining. To this effect, our data show that the ACSL1 deficiency dramatically suppressed intracellular lipid accumulation or foaming of macrophages, despite the PPAR-γ/δ -induced CD36 upregulation and short-term PA stimulation of these cells (Figures 4M and 4N). Taken together, these findings support the role of ACSL1 as a key regulator of lipid uptake and transport in macrophages and as a potential target to suppress inflammatory signaling involving the CD36/FAPB4/PLIN2 axis.

Inhibition of ACSL1 suppresses the short-term PA stimulation-induced inflammatory and lipid uptake responses in human PBMCs

Although continuous cell lines proliferate faster and indefinitely and are easier to work with, their functional integrity and physiology can be affected due to the genetic drift resulting from continuous passaging. Given that, primary cells provide more relevancy to conduct biomedical research and present an excellent *ex vivo* system for studying cellular physiology and biochemistry involving metabolic, signaling, and toxicity

studies. Therefore, the protective effects of ACSL1 inhibition were further evaluated using human PBMCs. In line with our data using THP-1-derived macrophages, pretreatment of human PBMCs with triacsin C also induced protective effects about inflammatory and lipid uptake responses. Flow cytometry analysis of triacsin C-treated human PBMCs, following short-term PA stimulation, showed a significant reduction ($p < 0.0001$) in the $CD14^{+}CD11b^{+}CD11c^{+}$ inflammatory subset, compared to controls (Figures 5A and 5B). As expected, it was also observed that pretreatment with triacsin C significantly reduced the lipid content within these pro-inflammatory cells (Figure 5C). Concomitantly, ACSL1 inhibition also led to the suppression of both CD36 ($p < 0.0001$) and FABP4 ($p < 0.05$) expression in this inflammatory subset (Figures 5D and 5E). Together, human PBMCs' data recapitulate the previous findings using THP-1-derived macrophages, verifying the key role of ACSL1 in regulating lipid accumulation and inflammatory responses via the CD36/FABP4 mediated signaling.

ACSL1 inhibition protects against the AHFF-induced inflammatory and lipid uptake responses in mice

To evaluate the therapeutic effect of ACSL1 inhibition in preventing AHFF-induced inflammatory response, fractalkine/CX3CL1 expression was assessed in circulatory monocytes using C57BL/6J mouse model. Both fractalkine/CX3CL1 chemokine and its receptor CXCR1 have been implicated with diet-induced inflammation and atherosclerotic lesion formation due to redirected homing of the circulatory proinflammatory monocytes to the target tissues.[32,33] As depicted in the schematic (Figure 6A), overnight-fasted C57BL/6J male mice, 8-9 weeks old, were orally administered vehicle (n = 5) or triacsin C (10 mg/kg body weight; n = 5)[34] by oral gavage and the mice were allowed to rest for 30 min before HFD feeding (30 g; 58 kcal% from fat). Blood samples were drawn at baseline (fasting state) and after 4 h of HFD feeding for flow cytometry analysis of CX3CL1 expression on activated monocytes in the circulation. As the data show, AHFF induced a significant increase in the activated $CD11b^{+}CD11c^{+}CX3CL1^{high}$ monocyte subset in the circulation in vehicle-treated mice, while no significant change in this inflammatory monocyte subset was observed in triacsin C-treated mice, suggesting an immunoprotective, anti-inflammatory effect of ACSL1 inhibition *in vivo* (Figures 6B–6D). Since the ACSL1 disruption in cultured macrophages was found to down-modulate FABP4 and PLIN2 expression and interrupt the lipid accumulation signaling downstream of CD36, we wondered if this beneficial effect was reproducible in the *in vivo* mouse model as well. To this end, isolated PBMCs showed significantly lower expression of FABP4 and PLIN2, and reduced p38 phosphorylation in triacsin C-treated mice compared with vehicle-treated controls (Figures 6E–6H). As supported by these data, ACSL1 inhibition in mice leads to suppression of both inflammatory and lipid uptake responses in the blood, suggesting that targeting ACSL1 lipid metabolic enzyme in macrophages may represent a strategy to reduce lipotoxicity and attenuate pathologic inflammation in metabolic disease.

DISCUSSION

The interplay between cellular metabolic pathways, lipotoxicity, and metabolic reprogramming in macrophages remains poorly understood. Herein, first, we show that the short-term stimulation of macrophages with PA for 4h, mimicking the effect of a single dose of AHFF, promotes the ACSL enzymatic activity. Free long-chain fatty acids (12-20 carbons) are known to be taken up by cells and converted into their acyl-CoA derivatives by a group of ACSLs comprising ACSL1, ACSL3, ACSL4, ACSL5, and ACSL6.[35] Each of these ACSL isoforms has distinct substrate specificities, cell type or tissue specific expression patterns, and different subcellular localizations.[36] Of the five ACSL isoforms reported, only ACSL1 and ACSL3 transcripts were found to be upregulated in these macrophages in response to short-term PA stimulation. Notably, ACSL1 among other isoforms herein tested, had the highest gene induction in macrophages, following a short-term PA stimulation which justifies the relevancy for further investigations of ACSL1 in these cells in our study. In line with this finding, transcriptional upregulation of ACSL1 was described in neutrophil cultures that were exposed *in vitro* to plasma from septic patients.[37] Several other studies also substantiate the functional role of ACSL1 in inflammatory responses involving macrophages.[38,39] A cell type can typically express several ACSL isoforms which can channel acyl-CoAs to various fates, such as neutral lipid storage or β oxidation.[40] Corroborating our findings with macrophages, other studies also reported that ACSL1 activity was correlated with the uptake of long-chain fatty acids[41]; while overexpression of ACSL1 led to the increased triglycerides accumulation in HepG2 cells.[42]

For being the most highly expressed member of the ACSL family in blood, ACSL1 is speculated to play a relatively more conspicuous role in immune responses compared to other ACSL family members. Importantly, we found that ACSL1 upregulation at the transcriptional and translational levels in response to

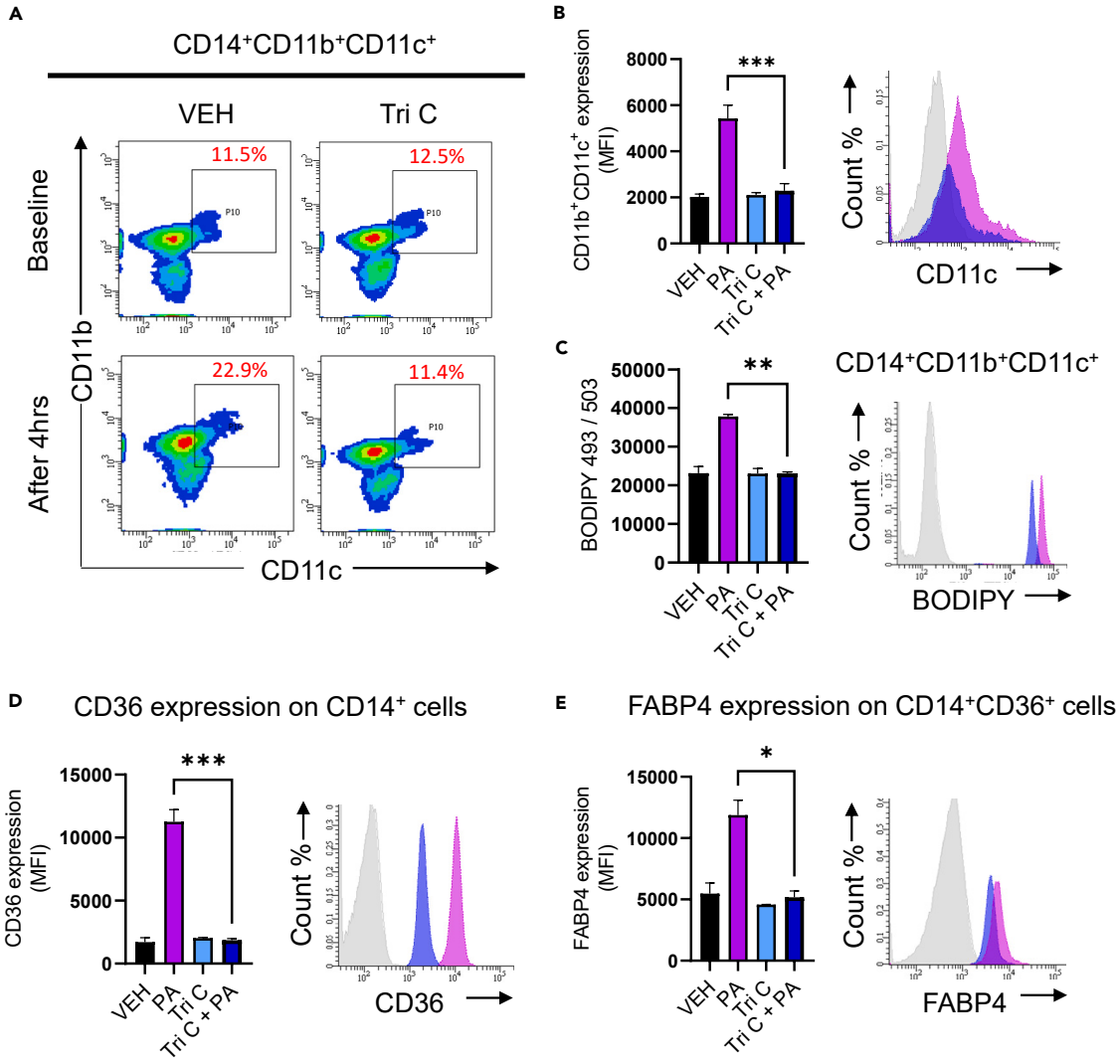

Figure 5. ACSL1 Inhibition attenuates the short-term palmitic acid (PA) stimulation-induced inflammatory and lipid uptake responses in primary human monocytes

Peripheral blood mononuclear cells (PBMC) were isolated from healthy donors' blood and primary monocytes ($CD14^+$ cells) were enriched by negative selection as described in STAR Methods. For ACSL1 inhibition studies, primary monocytes were first treated with triacsin C (5 μM; T4540) for 30-60 min and then stimulated with PA (150 μM) for 4 h at 37°C, while controls were treated with vehicle (0.1% BSA) only. For flow cytometry assays, cells were immunolabeled with fluorescent antibodies against markers of interest including CD14, CD11b, CD11c, BODIPY, CD36, and FABP4, following the manufacturers' instructions.

(A) Representative dot blots showing lower co-expression of CD11b+CD11c+, following short-term PA stimulation of triacsin C-treated primary human monocytes compared to controls treated with PA only.

(B) Flow cytometry analysis of inflammatory markers with representative overlayed histograms, displaying reduced surface co-expression of CD11b and CD11c, following short-term PA stimulation of triacsin C-treated primary human monocytes compared to controls treated with PA only.

(C) Flow cytometry analysis of BODIPY 493/503 staining with representative histograms, indicating the reduced intracellular lipids ACSL1-deficient primary human monocytes compared to controls treated with PA only.

(D) Flow cytometry analysis of CD36, with representative histograms, showing reduced CD36 expression in triacsin C-treated primary human monocytes following short-term PA stimulation compared to controls stimulated with PA only.

(E) Flow cytometry analysis of FABP4 with representative histograms, showing reduced intracellular FABP4 expression in triacsin C-treated primary human monocytes following short-term PA stimulation compared to controls stimulated with PA only. Data are presented as mean ± SEM (n = 3-5) and were analyzed using one-way ANOVA with Tukey's test. *$p \leq 0.05$, ***$p \leq 0.001$.

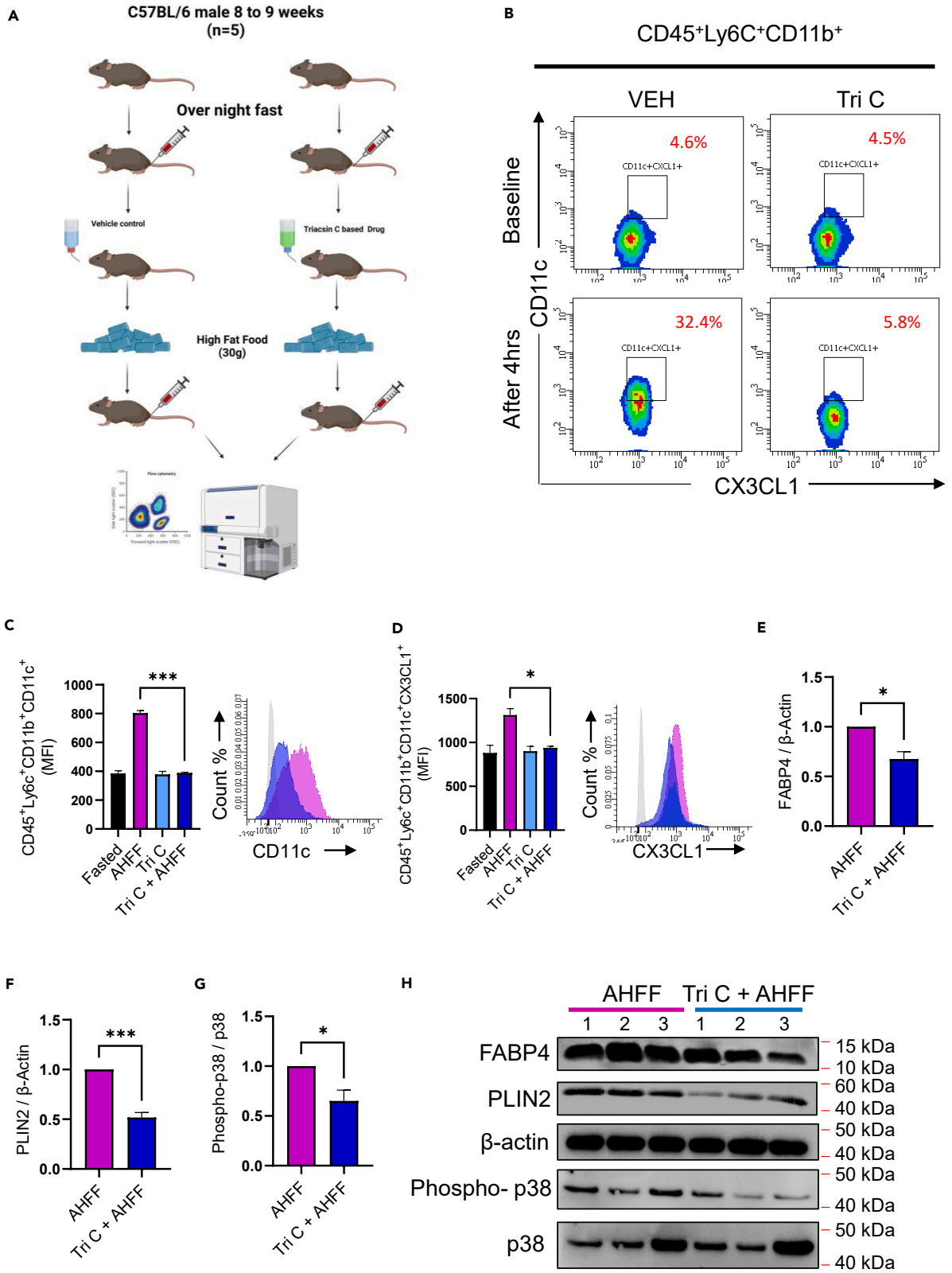
A
C57BL/6 male 8 to 9 weeks
(n=5)
Over night fast
Vehicle control
Triacsin C based Drug
High Fat Food
(30g)
B
CD45+Ly6C+CD11b+
VEH
Tri C
Baseline
After 4hrs
CD11c
CX3CL1
4.6%
4.5%
32.4%
5.8%
CD11c+CXCL1+
C
CD45+Ly6c+CD11b+CD11c+
(MFI)
***
Fasted
AHFF
Tri C
Tri C + AHFF
Count %
CD11c
D
CD45+Ly6c+CD11b+CD11c+CX3CL1+
(MFI)
*
CX3CL1
E
FABP4 / β-Actin
F
PLIN2 / β-Actin
G
Phospho-p38 / p38
H
AHFF
Tri C + AHFF
FABP4
PLIN2
β-actin
Phospho- p38
p38
15 kDa
10 kDa
60 kDa
40 kDa
50 kDa
40 kDa
50 kDa
40 kDa
50 kDa
40 kDa

Figure 6. ACSL1 inhibition protects against the short-term high-fat feeding (AHFF)-induced inflammatory responses in mice

Overnight-fasted mice were administered triacsin C (10 mg/kg) or vehicle by oral gavage. After 30 min, mice were fed high-fat diet (58% kcal from fat; 30g) and blood samples (50-60μL each) were drawn for analysis, before and 4 h after triacsin C administration.

(A) A schematic diagram showing the *in vivo* study design.

(B) Representative dot blots from flow cytometry analysis of CD45+Ly6C + CD11b+ cell population showing reduced CD11c+CX3CL1+ co-expression on blood monocytes following the AHFF of triacsin C-administered mice compared to untreated control mice.

(C-G) Flow cytometry analysis for monocyte/macrophage inflammatory markers with representative histograms, depicting reduced expression of CD11c and CX3CL1 on CD45+Ly6C+ monocytes from triacsin C-administered mice compared to control mice, following an AHFF dietary challenge. Immunoblot quantification data analysis showing reduced expression of (E and F) FABP4 and PLIN2 proteins and (G) reduced phosphorylation of p38 MAPK in blood monocytes isolated from triacsin C-administered mice compared to control mice, following an AHFF dietary challenge.

(H) Representative immunoblots displaying a diminished expression of FABP4, PLIN2, and p-p38 in blood monocytes from triacsin C-treated mice compared to control mice, following an AHFF dietary challenge. 3 biological replicates were used for western blot quantification. Data were presented as mean ± SEM (n = 4-5 mice per group) and were analyzed by using one-way ANOVA with Tukey's test *p ≤ 0.05, ***p ≤ 0.001.

short-term PA stimulation associated with the intracellular lipid accumulation and secretion of typical M1 pro-inflammatory cytokines/chemokine including TNF-α, IL-1β, and MCP-1. These findings suggest that the short-term palmitate stimulation, which mimics the early stage of AHFF, could drive monocytic cell transformation into the lipid-laden pro-inflammatory M1 macrophages, also known as foam cells. This lipid-driven foam cell formation is known as an underlying mechanism driving the pathophysiology of disorders associated with metabolic syndromes, such as obesity, cardiovascular disease, T2D, and atherosclerosis.[11,43] Several studies, including ours, point to the potential link between ACSL1 upregulation and induction of inflammatory macrophage M1 phenotype in a metabolic disease setting, further showing that ACSL1 pharmaceutical inhibition or gene silencing leads to effective suppression of the ACSL1-driven inflammatory responses.[16,39,44–46] To this end, it remains unclear how ACSL1 inhibition or silencing may impact the lipid accumulation and foam cell transformation in macrophages, following a short-term (4 h) exposure to palmitate to recapitulate the AHFF conditions. We herein report that ACSL1 inhibition or genetic silencing suppresses expression of lipid scavenger receptor CD36 and fatty acid transporter protein FABP4, preventing lipid uptake and accumulation, however, with no significant effects on fatty acid oxidation and lipogenesis.

Regarding whether ACSL1 inhibition or deficiency was more effective pre- or post-PA stimulation, we found that ACSL1 inhibition post-PA stimulation had no significant effect on intracellular lipid accumulation in the transformed macrophages, implying that ACSL1 inhibition in a clinical setting could be more advantageous during early stages of AHFF for preventing the pathophysiological effects downstream of CD36 signaling, such as lipid uptake and accumulation, M1 macrophage polarization, and inflammatory responses.

The molecular mechanisms regulating the uptake of long-chain fatty acids are still debated. A clear understanding of these processes is important for identifying potential targets for treating lipid disorders. The initial step involved in long-chain fatty acids uptake is their translocation across the plasma membrane, perhaps through the mechanism of facilitated uptake. In this regard, CD36 scavenger protein has been shown to be consistently expressed at the plasma membrane and its overexpression was found to associate with increased long-chain fatty acids uptake.[47] CD36 is a pattern recognition receptor expressed on various cells and tissue and is a central player in sensing, importing, and metabolising lipids and free fatty acids in these cells and tissues. CD36 binds multiple ligands, such as fatty acids, phospholipids, acetylated LDL, and collagen, and it mediates different biological processes including metabolism, angiogenesis, immunity, and behavior.[48,49] CD36 is located in both lipid raft and non-lipid raft domains of the plasma membrane and facilitates lipid uptake by accumulating long-chain fatty acids on the outer surface of the cellular plasma membrane.[50] CD36 was found to be involved in the progression of atherosclerosis while its genetic deletion or pharmaceutical inhibition effectively reduced the formation of atherosclerotic lesions.[51] Indeed, the short-term PA stimulation of transformed macrophages induced robust upregulation of macrophage inflammatory and adhesion marker proteins and we found that their expression was largely abolished after the pharmacological inhibition of ACSL1 using triacsin C or by siRNA-mediated ACSL1 gene silencing. We further demonstrated that ACSL1 inhibition or deficiency prevented the CD36 downstream MAPK signaling via p38 and JNK. Notably, MAPK signaling is involved in multiple biological processes such as survival, proliferation, differentiation, inflammation, apoptosis, and autophagy as well as it plays a key role in the pathogenesis of macrophage-mediated inflammatory diseases.[52] In line with our findings, mounting evidence corroborates that CD36 induction/upregulation and foam cell formation involves signaling via the p38 activation.[26,53,54]

Given that CD36 expression is transcriptionally regulated by a type II nuclear receptor PPARγ,[29,55] we investigated the expression of the PPAR isoforms in response to short-term PA treatment of cultured macrophages, reminiscing the AHFF effect on macrophages *in vivo*. Interestingly, out of the three known PPAR isoforms, only PPARδ expression was found to be significantly induced by short-term PA stimulation, and its expression was significantly downregulated either by inhibition or deficiency of ACSL1. Of note, CD36 has been generally recognized as a PPARγ target gene since the PPARγ-responsive element (PPRE) has been found in the proximal region of the CD36 promoter.[28,56] The emerging evidence, including our data, seems to be supporting the notion that other PPARs, such as PPARδ, may also regulate CD36-mediated lipid homeostasis by promoting fatty acid uptake, transport, and lipid droplet formation.[57] Similarly, another study by Nahle et al. showed that during the fasting state, activation of PPARδ subsequently upregulated the expression of CD36 to increase fatty acid utilization in the skeletal muscle.[58] In our study, we found that PPARδ activation by its agonist GW0742 led to a significant upregulation of CD36 in a similar manner while the PPARγ agonist rosiglitazone did not have such an effect, implying that in certain conditions, PPARδ might comparably regulate the CD36 expression in macrophages to control lipid homeostasis. Nevertheless, activation of both PPARδ and PPARγ was found to increase the ACSL1 enzymatic activity. Previous evidence points largely to the involvement of PPARγ in CD36 expression or induction and foam cell formation in macrophages[28,59] or in promoting foam cell-like morphologies in other cell types[60]; while Lee et al. report a ligand-dependent transcriptional pathway wherein PPARδ orchestrates the regulatory switch via its association and disassociation with transcriptional repressors and thus controls the macrophage inflammatory status and atherogenesis.[61]

Furthermore, regardless of the activation of PPARδ or CD36, ACSL1 lacking/defective macrophages had reduced expression of FABP4 and inflammatory mediators or markers. Our co-immunostaining analysis indicated that the expression of FABP4 and ACSL1 was interlinked. FABP4 is a member of the fatty acid-binding proteins (FABPs) family that acts as a chaperon molecule and transports fatty acids between cellular compartments. In normal conditions, both CD36 and FABP4 act in unison to maintain lipid homeostasis by regulating rates of fatty acid import and metabolism. FABPs play a critical role by ensuring that imported fatty acids are effectively shuttled to subcellular locations, a process that is catalyzed by ACSL1. Therefore, in the absence of ACSL1 enzymatic activity, lipid accumulation is abolished or reduced, even in the event of an induced activation of CD36. Our results suggest that the stimuli known to induce CD36-mediated activation of fatty acid uptake do not hamper the cooperativity between FABP4 and ACSL1. In this regard, our findings are more consistent with a model in which ACSL1 and FABP4 are driven by short-term PA stimulation to interact in a fundamental and stable manner in activated macrophages.

In order to gain a further insight into the regulatory role of ACSL1 in fatty acid homeostasis *in vivo*, we fed the overnight-fasted C57BL/6J mice with ASCL1 inhibitor triacsin C or with vehicle, 30 min prior to a single dose of HFD feeding in order to establish an AHFF model. After 4 h of HFD feeding, it became evident that in agreement with our *in vitro* studies, even at an early stage of AHFF, a shift in blood monocytes polarization occurred whereby over 25% circulatory monocytes were found to express a typical proinflammatory phenotype defined by the expression of $Ly6C^{high}CD11b^{+}CD11c^{+}CX3CL1^{+}$ surface markers. Interestingly, as expected, an oral dose of 10 mg/body weight of triacsin C in mice significantly blocked the activation of the inflammatory cascade through FABP4 blockade and effectively prevented foamy cell formation and reduced inflammatory signaling downstream of CD36, recapitulating similar effects in cultured macrophages that were subjected to short-term PA stimulation using an *in vitro* model approach.

In conclusion, addressing the core question of how AHFF may impact the macrophage-associated inflammatory responses, we found that following an short-term PA stimulation of transformed macrophages *in vitro* or during the early phase of HFD feeding in overnight-fasted mice, both the CD36 scavenger receptor and FABP4 fatty acid transport protein play key roles in fatty acid uptake, transport, lipid accumulation, and inflammatory activation, leading to foam cell formation, in a potential mechanism pivoted on the ACSL1 enzymatic activity. We also found a strong interaction between ACSL1 and FABP4, following the activation of CD36 either by short-term PA stimulation *in vitro* or during the early stage of AHFF *in vivo*. Moreover, synthetically induced PPARδ and PPARγ activation fails to upregulate the expression of FABP4 in the absence of a functional ACSL1 activity. Mechanistically, ACSL1 dysfunction in macrophages down modulates the p38-associated inflammatory signaling and suppresses lipid accumulation and foam cell formation, as illustrated in the schematic model (Figure 7).

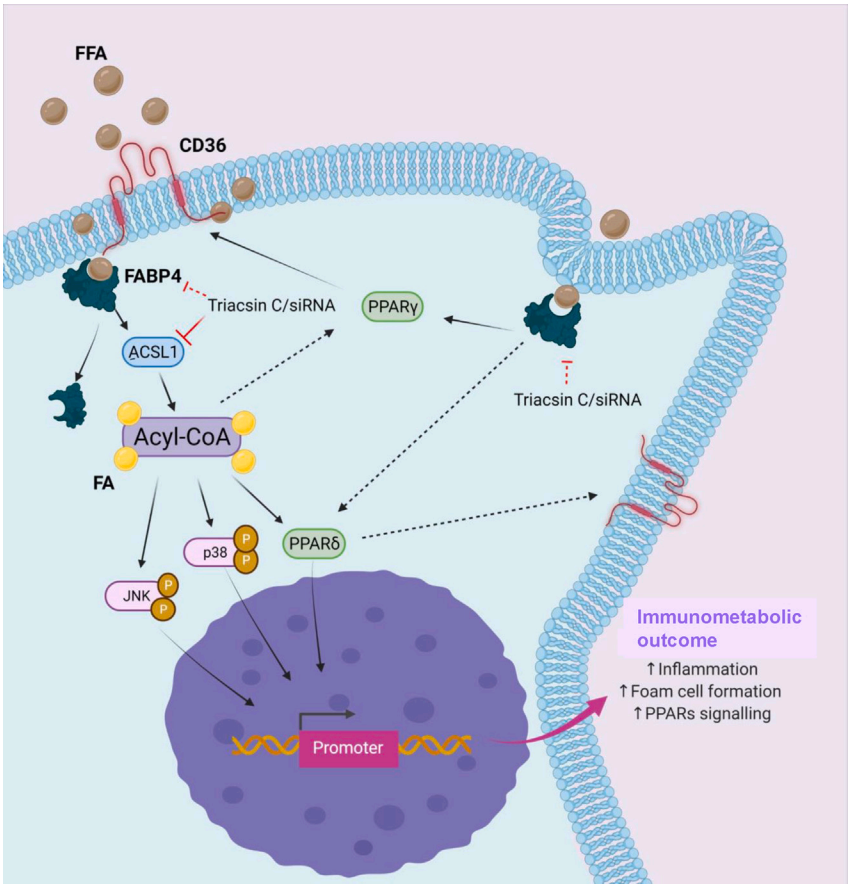

Figure 7. Schematic illustration of the key role of ACSL1 in inflammatory signaling and macrophage foaming, after short-term PA stimulation *in vitro* or a dietary challenge (AHFF) in a mouse model

Limitations of the study

We have shown that the activation of major nuclear factors PPARs and MAPKs are affected by ACSL1 inhibition. Although we have defined the CD36/FABP4 upstream pathway of PPARδ in this study and only investigated endpoint expression of MAPKs; p38 and JNK and were not able to establish a direct effect between PPARs and MAPKs. While our findings suggest a potential relationship between these signaling pathways, we did not directly investigate the mechanism of interaction between PPARs and MAPKs. Therefore, additional research will be needed to reveal the precise nature of this relationship.

STAR★METHODS

Detailed methods are provided in the online version of this paper and include the following:

- KEY RESOURCES TABLE
- RESOURCE AVAILABILITY
  - Lead contact
  - Materials availability
  - Data and code availability
- EXPERIMENTAL MODEL AND SUBJECT DETAILS
  - Cell culture
  - Isolation of human peripheral blood mononuclear cells (PBMC) and monocyte purification
  - Mice studies
- METHOD DETAILS
  - Cell stimulation

SUPPLEMENTAL INFORMATION

Supplemental information can be found online at https://doi.org/10.1016/j.isci.2023.107145.

ACKNOWLEDGMENTS

The authors would also like to thank all animal technical staff for the essential husbandry work with our animal models. This work was supported by the Kuwait Foundation for the Advancement of Sciences Grant RA-CB 2020-004 (to R.A. and FAR.) and National Institutes of Health Grant P01 CA97132 (to Y.A.H.). The funders had no role in the study design; collection, analysis, and interpretation of data; writing of this paper; or in the decision to submit the paper for publication.

AUTHOR CONTRIBUTIONS

Conceptualization, F.A.R., L.M.O., Y.A.H., and R.A.; methodology, F.A.R., and R.A.; investigation, F.A.R., D.H., A.A.M., T.J, and S.K.; formal Analysis, F.A.R., A.A.M., and S.S.; writing – original draft, F.A.R.; writing – review & editing, S.S., F.A.M, Y.A.H., and R.A.; funding acquisition, F.A.R., Y.A.H., and R.A.; resources, F.A.M., and R.A.; supervision, R.A. All authors contributed to reviewing the paper and all authors have read and approved the final version for submission.

DECLARATION OF INTERESTS

The authors declare that they have no competing interests.

Received: September 9, 2022
Revised: April 29, 2023
Accepted: June 12, 2023
Published: June 15, 2023

REFERENCES

1. Koca, N., Ayar, K., Bal, Ö., and Ersoy, C. (2021). The evaluation of the role of BMI and insulin resistance on inflammatory markers, PAI-1 levels and arterial stiffness in newly diagnosed type 2 diabetes mellitus patients. Minerva Endocrinol. *46*, 116–123. https://doi.org/10.23736/S2724-6507.20.03158-2.

2. Feng, Y., Cirera, S., Taşöz, E., Liu, Y., Olsen, L.H., Christoffersen, B.Ø., Pedersen, H.D., Ludvigsen, T.P., Kirk, R.K., Schumacher-Petersen, C., et al. (2021). Diet-Dependent Changes of the DNA Methylome Using a Göttingen Minipig Model for Obesity. Front. Genet. *12*, 632859. https://doi.org/10.3389/fgene.2021.632859.

3. Pikó, P., Pál, L., Szűcs, S., Kósa, Z., Sándor, J., and Ádány, R. (2021). Obesity-Related Changes in Human Plasma Lipidome Determined by the Lipidyzer Platform. Biomolecules *11*, 326. https://doi.org/10.3390/biom11020326.

4. Moore, K.J., and Tabas, I. (2011). Macrophages in the pathogenesis of atherosclerosis. Cell *145*, 341–355. https://doi.org/10.1016/j.cell.2011.04.005.

5. Simons, K., and Ikonen, E. (2000). How cells handle cholesterol. Science *290*, 1721–1726. https://doi.org/10.1126/science.290.5497.1721.

6. Wang, L., Gill, R., Pedersen, T.L., Higgins, L.J., Newman, J.W., and Rutledge, J.C. (2009). Triglyceride-rich lipoprotein lipolysis releases neutral and oxidized FFAs that induce endothelial cell inflammation. J. Lipid Res. *50*, 204–213. https://doi.org/10.1194/jlr.M700505-JLR200.

7. Wang, Y., You, Y., Tian, Y., Sun, H., Li, X., Wang, X., Wang, Y., and Liu, J. (2020). PP04 Ameliorates High-Fat Diet-Induced Hyperlipidemia by Regulating Lipid Metabolism in C57BL/6N Mice. J. Agric. Food Chem. *68*, 15154–15163. https://doi.org/10.1021/acs.jafc.0c05060.

8. Henning, A.L., Venable, A.S., Vingren, J.L., Hill, D.W., and McFarlin, B.K. (2018). Consumption of a high-fat meal was associated with an increase in monocyte adhesion molecules, scavenger receptors, and Propensity to Form Foam Cells. Cytometry B Clin. Cytom. *94*, 606–612. https://doi.org/10.1002/cyto.b.21478.

9. Poznyak, A.V., Nikiforov, N.G., Starodubova, A.V., Popkova, T.V., and Orekhov, A.N. (2021). Macrophages and Foam Cells: Brief Overview of Their Role, Linkage, and Targeting Potential in Atherosclerosis. Biomedicines *9*, 1221. https://doi.org/10.3390/biomedicines9091221.

10. Kim, S., Cho, W., Kim, I., Lee, S.H., Oh, G.T., and Park, Y.M. (2020). Oxidized LDL induces vimentin secretion by macrophages and contributes to atherosclerotic inflammation. J. Mol. Med. *98*, 973–983. https://doi.org/10.1007/s00109-020-01923-w.

11. Filipek, A., Mikołajczyk, T.P., Guzik, T.J., and Naruszewicz, M. (2020). Oleacein and Foam Cell Formation in Human Monocyte-Derived Macrophages: A Potential Strategy Against Early and Advanced Atherosclerotic Lesions. Pharmaceuticals *13*, 64. https://doi.org/10.3390/ph13040064.

12. Hao, J.W., Wang, J., Guo, H., Zhao, Y.Y., Sun, H.H., Li, Y.F., Lai, X.Y., Zhao, N., Wang, X., Xie, C., et al. (2020). CD36 facilitates fatty acid uptake by dynamic palmitoylation-regulated endocytosis. Nat. Commun. *11*, 4765. https://doi.org/10.1038/s41467-020-18565-8.

13. Coleman, R.A. (2019). It takes a village: channeling fatty acid metabolism and triacylglycerol formation via protein interactomes. J. Lipid Res. *60*, 490–497. https://doi.org/10.1194/jlr.S091843.

14. Klett, E.L., Chen, S., Yechoor, A., Lih, F.B., and Coleman, R.A. (2017). Long-chain acyl-CoA synthetase isoforms differ in preferences for eicosanoid species and long-chain fatty acids. J. Lipid Res. *58*, 884–894. https://doi.org/10.1194/jlr.M072512.

15. Killion, E.A., Reeves, A.R., El Azzouny, M.A., Yan, Q.W., Surujon, D., Griffin, J.D., Bowman, T.A., Wang, C., Matthan, N.R., Klett, E.L., et al. (2018). A role for long-chain acyl-CoA synthetase-4 (ACSL4) in diet-induced phospholipid remodeling and obesity-associated adipocyte dysfunction. Mol. Metabol. *9*, 43–56. https://doi.org/10.1016/j.molmet.2018.01.012.

16. Al-Rashed, F., Ahmad, Z., Iskandar, M.A., Tuomilehto, J., Al-Mulla, F., and Ahmad, R. (2019). TNF-α Induces a Pro-Inflammatory Phenotypic Shift in Monocytes through ACSL1: Relevance to Metabolic Inflammation. Cell. Physiol. Biochem. *52*, 397–407. https://doi.org/10.33594/000000028.

17. Kuwata, H., Yoshimura, M., Sasaki, Y., Yoda, E., Nakatani, Y., Kudo, I., and Hara, S. (2014). Role of long-chain acyl-coenzyme A synthetases in the regulation of arachidonic acid metabolism in interleukin 1β-stimulated rat fibroblasts. Biochim. Biophys. Acta *1841*, 44–53. https://doi.org/10.1016/j.bbalip.2013.09.015.

18. Grevengoed, T.J., Klett, E.L., and Coleman, R.A. (2014). Acyl-CoA metabolism and partitioning. Annu. Rev. Nutr. *34*, 1–30. https://doi.org/10.1146/annurev-nutr-071813-105541.

19. Roelands, J., Garand, M., Hinchcliff, E., Ma, Y., Shah, P., Toufiq, M., Alfaki, M., Hendrickx, W., Boughorbel, S., Rinchai, D., et al. (2019). Long-Chain Acyl-CoA Synthetase 1 Role in Sepsis and Immunity: Perspectives From a Parallel Review of Public Transcriptome Datasets and of the Literature. Front. Immunol. *10*, 2410. https://doi.org/10.3389/fimmu.2019.02410.

20. Schmid, A., Petry, N., Walther, B., Bütikofer, U., Luginbühl, W., Gille, D., Chollet, M., McTernan, P.G., Gijs, M.A.M., Vionnet, N., et al. (2015). Inflammatory and metabolic responses to high-fat meals with and without dairy products in men. Br. J. Nutr. *113*, 1853–1861. https://doi.org/10.1017/S0007114515000677.

21. Fatima, S., Hu, X., Huang, C., Zhang, W., Cai, J., Huang, M., Gong, R.H., Chen, M., Ho, A.H.M., Su, T., et al. (2019). High-fat diet feeding and palmitic acid increase CRC growth in β2AR-dependent manner. Cell Death Dis. *10*, 711. https://doi.org/10.1038/s41419-019-1958-6.

22. Myhrstad, M.C.W., Narverud, I., Telle-Hansen, V.H., Karhu, T., Lund, D.B., Herzig, K.H., Makinen, M., Halvorsen, B., Retterstøl, K., Kirkhus, B., et al. (2011). Effect of the fat composition of a single high-fat meal on inflammatory markers in healthy young women. Br. J. Nutr. *106*, 1826–1835. https://doi.org/10.1017/S0007114511002510.

23. Kageyama, A., Matsui, H., Ohta, M., Sambuichi, K., Kawano, H., Notsu, T., Imada, K., Yokoyama, T., and Kurabayashi, M. (2013). Palmitic acid induces osteoblastic differentiation in vascular smooth muscle cells through ACSL3 and NF-κB, novel targets of eicosapentaenoic acid. PLoS One *8*, e68197. https://doi.org/10.1371/journal.pone.0068197.

24. Cai, L., Wang, Z., Ji, A., Meyer, J.M., and van der Westhuyzen, D.R. (2012). Scavenger receptor CD36 expression contributes to adipose tissue inflammation and cell death in diet-induced obesity. PLoS One *7*, e36785. https://doi.org/10.1371/journal.pone.0036785.

25. Garin-Shkolnik, T., Rudich, A., Hotamisligil, G.S., and Rubinstein, M. (2014). FABP4 attenuates PPARγ and adipogenesis and is inversely correlated with PPARγ in adipose tissues. Diabetes *63*, 900–911. https://doi.org/10.2337/db13-0436.

26. Zhao, M., Liu, Y., Wang, X., New, L., Han, J., and Brunk, U.T. (2002). Activation of the p38 MAP kinase pathway is required for foam cell formation from macrophages exposed to oxidized LDL. APMIS *110*, 458–468. https://doi.org/10.1034/j.1600-0463.2002.100604.x.

27. Rigamonti, E., Chinetti-Gbaguidi, G., and Staels, B. (2008). Regulation of macrophage functions by PPAR-alpha, PPAR-gamma, and LXRs in mice and men. Arterioscler. Thromb. Vasc. Biol. *28*, 1050–1059. https://doi.org/10.1161/ATVBAHA.107.158998.

28. Maréchal, L., Laviolette, M., Rodrigue-Way, A., Sow, B., Brochu, M., Caron, V., and Tremblay, A. (2018). The CD36-PPARγ Pathway in Metabolic Disorders. Int. J. Mol. Sci. *19*, 1529. https://doi.org/10.3390/ijms19051529.

29. Yang, X., Zhang, W., Chen, Y., Li, Y., Sun, L., Liu, Y., Liu, M., Yu, M., Li, X., Han, J., and Duan, Y. (2016). Activation of Peroxisome Proliferator-activated Receptor γ (PPARγ) and CD36 Protein Expression: THE DUAL PATHOPHYSIOLOGICAL ROLES OF PROGESTERONE. J. Biol. Chem. *291*, 15108–15118. https://doi.org/10.1074/jbc.M116.726737.

30. Wilfling, F., Wang, H., Haas, J.T., Krahmer, N., Gould, T.J., Uchida, A., Cheng, J.X., Graham, M., Christiano, R., Fröhlich, F., et al. (2013). Triacylglycerol synthesis enzymes mediate lipid droplet growth by relocalizing from the ER to lipid droplets. Dev. Cell *24*, 384–399. https://doi.org/10.1016/j.devcel.2013.01.013.

31. Brasaemle, D.L., Dolios, G., Shapiro, L., and Wang, R. (2004). Proteomic analysis of proteins associated with lipid droplets of basal and lipolytically stimulated 3T3-L1 adipocytes. J. Biol. Chem. *279*, 46835–46842. https://doi.org/10.1074/jbc.M409340200.

32. Jones, B.A., Beamer, M., and Ahmed, S. (2010). Fractalkine/CX3CL1: a potential new target for inflammatory diseases. Mol. Interv. *10*, 263–270. https://doi.org/10.1124/mi.10.5.3.

33. Riopel, M., Vassallo, M., Ehinger, E., Pattison, J., Bowden, K., Winkels, H., Wilson, M., de Jong, R., Patel, S., Balakrishna, D., et al. (2019). CX3CL1-Fc treatment prevents atherosclerosis in Ldlr KO mice. Mol. Metabol. *20*, 89–101. https://doi.org/10.1016/j.molmet.2018.11.011.

34. Matsuda, D., Namatame, I., Ohshiro, T., Ishibashi, S., Omura, S., and Tomoda, H. (2008). Anti-atherosclerotic activity of triacsin C, an acyl-CoA synthetase inhibitor. J. Antibiot. *61*, 318–321. https://doi.org/10.1038/ja.2008.45.

35. Mashek, D.G., Bornfeldt, K.E., Coleman, R.A., Berger, J., Bernlohr, D.A., Black, P., DiRusso, C.C., Farber, S.A., Guo, W., Hashimoto, N., et al. (2004). Revised nomenclature for the mammalian long-chain acyl-CoA synthetase gene family. J. Lipid Res. *45*, 1958–1961. https://doi.org/10.1194/jlr.E400002-JLR200.

36. Mashek, D.G., Li, L.O., and Coleman, R.A. (2007). Long-chain acyl-CoA synthetases and fatty acid channeling. Future Lipidol. *2*, 465–476. https://doi.org/10.2217/17460875.2.4.465.

37. Khaenam, P., Rinchai, D., Altman, M.C., Chiche, L., Buddhisa, S., Kewcharoenwong, C., Suwannasaen, D., Mason, M., Whalen, E., Presnell, S., et al. (2014). A transcriptomic reporter assay employing neutrophils to measure immunogenic activity of septic patients' plasma. J. Transl. Med. *12*, 65. https://doi.org/10.1186/1479-5876-12-65.

38. Rubinow, K.B., Wall, V.Z., Nelson, J., Mar, D., Bomsztyk, K., Askari, B., Lai, M.A., Smith, K.D., Han, M.S., Vivekanandan-Giri, A., et al. (2013). Acyl-CoA synthetase 1 is induced by Gram-negative bacteria and lipopolysaccharide and is required for phospholipid turnover in stimulated macrophages. J. Biol. Chem. *288*, 9957–9970. https://doi.org/10.1074/jbc.M113.458372.

39. Kanter, J.E., Kramer, F., Barnhart, S., Averill, M.M., Vivekanandan-Giri, A., Vickery, T., Li, L.O., Becker, L., Yuan, W., Chait, A., et al. (2012). Diabetes promotes an inflammatory macrophage phenotype and atherosclerosis through acyl-CoA synthetase 1. Proc. Natl. Acad. Sci. USA *109*, E715–E724. https://doi.org/10.1073/pnas.1111600109.

40. Cooper, D.E., Young, P.A., Klett, E.L., and Coleman, R.A. (2015). Physiological Consequences of Compartmentalized

Acyl-CoA Metabolism. J. Biol. Chem. *290*, 20023–20031. https://doi.org/10.1074/jbc.R115.663260.

41. Milger, K., Herrmann, T., Becker, C., Gotthardt, D., Zickwolf, J., Ehehalt, R., Watkins, P.A., Stremmel, W., and Füllekrug, J. (2006). Cellular uptake of fatty acids driven by the ER-localized acyl-CoA synthetase FATP4. J. Cell Sci. *119*, 4678–4688. https://doi.org/10.1242/jcs.03280.

42. Parkes, H.A., Preston, E., Wilks, D., Ballesteros, M., Carpenter, L., Wood, L., Kraegen, E.W., Furler, S.M., and Cooney, G.J. (2006). Overexpression of acyl-CoA synthetase-1 increases lipid deposition in hepatic (HepG2) cells and rodent liver in vivo. Am. J. Physiol. Endocrinol. Metab. *291*, E737–E744. https://doi.org/10.1152/ajpendo.00112.2006.

43. Bobryshev, Y.V. (2006). Monocyte recruitment and foam cell formation in atherosclerosis. Micron *37*, 208–222. https://doi.org/10.1016/j.micron.2005.10.007.

44. Al-Rashed, F., Thomas, R., Al-Roub, A., Al-Mulla, F., and Ahmad, R. (2020). LPS Induces GM-CSF Production by Breast Cancer MDA-MB-231 Cells via Long-Chain Acyl-CoA Synthetase 1. Molecules *25*, 4709. https://doi.org/10.3390/molecules25204709.

45. Thomas, R., Al-Rashed, F., Akhter, N., Al-Mulla, F., and Ahmad, R. (2019). ACSL1 Regulates TNFα-Induced GM-CSF Production by Breast Cancer MDA-MB-231 Cells. Biomolecules *9*, 555. https://doi.org/10.3390/biom9100555.

46. Chang, Y.S., Tsai, C.T., Huangfu, C.A., Huang, W.Y., Lei, H.Y., Lin, C.F., Su, I.J., Chang, W.T., Wu, P.H., Chen, Y.T., et al. (2011). ACSL3 and GSK-3β are essential for lipid upregulation induced by endoplasmic reticulum stress in liver cells. J. Cell. Biochem. *112*, 881–893. https://doi.org/10.1002/jcb.22996.

47. Su, X., and Abumrad, N.A. (2009). Cellular fatty acid uptake: a pathway under construction. Trends Endocrinol. Metabol. *20*, 72–77. https://doi.org/10.1016/j.tem.2008.11.001.

48. Connelly, M.A., Klein, S.M., Azhar, S., Abumrad, N.A., and Williams, D.L. (1999). Comparison of class B scavenger receptors, CD36 and scavenger receptor BI (SR-BI), shows that both receptors mediate high density lipoprotein-cholesteryl ester selective uptake but SR-BI exhibits a unique enhancement of cholesteryl ester uptake. J. Biol. Chem. *274*, 41–47. https://doi.org/10.1074/jbc.274.1.41.

49. Silverstein, R.L., and Febbraio, M. (2009). CD36, a scavenger receptor involved in immunity, metabolism, angiogenesis, and behavior. Sci. Signal. *2*, re3. https://doi.org/10.1126/scisignal.272re3.

50. Ehehalt, R., Sparla, R., Kulaksiz, H., Herrmann, T., Füllekrug, J., and Stremmel, W. (2008). Uptake of long chain fatty acids is regulated by dynamic interaction of FAT/CD36 with cholesterol/sphingolipid enriched microdomains (lipid rafts). BMC Cell Biol. *9*, 45. https://doi.org/10.1186/1471-2121-9-45.

51. Park, Y.M. (2014). CD36, a scavenger receptor implicated in atherosclerosis. Exp. Mol. Med. *46*, e99. https://doi.org/10.1038/emm.2014.38.

52. Yang, Y., Kim, S.C., Yu, T., Yi, Y.S., Rhee, M.H., Sung, G.H., Yoo, B.C., and Cho, J.Y. (2014). Functional roles of p38 mitogen-activated protein kinase in macrophage-mediated inflammatory responses. Mediat. Inflamm. *2014*, 352371. https://doi.org/10.1155/2014/352371.

53. Wang, J., Feng, M.J., Zhang, R., Yu, D.M., Zhou, S.J., Chen, R., and Yu, P. (2016). Creactive protein/oxidized low density lipoprotein/beta2glycoprotein i complexes induce lipid accumulation and inflammatory reaction in macrophages via p38/mitogenactivated protein kinase and nuclear factorkappaB signaling pathways. Mol. Med. Rep. *14*, 3490–3498. https://doi.org/10.3892/mmr.2016.5622.

54. Min, K.J., Um, H.J., Cho, K.H., and Kwon, T.K. (2013). Curcumin inhibits oxLDL-induced CD36 expression and foam cell formation through the inhibition of p38 MAPK phosphorylation. Food Chem. Toxicol. *58*, 77–85. https://doi.org/10.1016/j.fct.2013.04.008.

55. Ballesteros, I., Cuartero, M.I., Pradillo, J.M., de la Parra, J., Pérez-Ruiz, A., Corbí, A., Ricote, M., Hamilton, J.A., Sobrado, M., Vivancos, J., et al. (2014). Rosiglitazone-induced CD36 up-regulation resolves inflammation by PPARγ and 5-LO-dependent pathways. J. Leukoc. Biol. *95*, 587–598. https://doi.org/10.1189/jlb.0613326.

56. Liu, J., Zhao, H., Yang, L., Wang, X., Yang, L., Xing, Y., Lv, X., Ma, H., and Song, G. (2022). The role of CD36-Fabp4-PPARγ in skeletal muscle involves insulin resistance in intrauterine growth retardation mice with catch-up growth. BMC Endocr. Disord. *22*, 10. https://doi.org/10.1186/s12902-021-00921-4.

57. Shi, H.B., Zhang, C.H., Xu, Z.A., Lou, G.G., Liu, J.X., Luo, J., and Loor, J.J. (2018). Peroxisome proliferator-activated receptor delta regulates lipid droplet formation and transport in goat mammary epithelial cells. J. Dairy Sci. *101*, 2641–2649. https://doi.org/10.3168/jds.2017-13543.

58. Nahlé, Z., Hsieh, M., Pietka, T., Coburn, C.T., Grimaldi, P.A., Zhang, M.Q., Das, D., and Abumrad, N.A. (2008). CD36-dependent regulation of muscle FoxO1 and PDK4 in the PPAR delta/beta-mediated adaptation to metabolic stress. J. Biol. Chem. *283*, 14317–14326. https://doi.org/10.1074/jbc.M706478200.

59. Tontonoz, P., Nagy, L., Alvarez, J.G., Thomazy, V.A., and Evans, R.M. (1998). PPARgamma promotes monocyte/macrophage differentiation and uptake of oxidized LDL. Cell *93*, 241–252. https://doi.org/10.1016/s0092-8674(00)81575-5.

60. Lim, H.J., Lee, S., Lee, K.S., Park, J.H., Jang, Y., Lee, E.J., and Park, H.Y. (2006). PPARgamma activation induces CD36 expression and stimulates foam cell like changes in rVSMCs. Prostag. Other Lipid Mediat. *80*, 165–174. https://doi.org/10.1016/j.prostaglandins.2006.06.006.

61. Lee, C.H., Chawla, A., Urbiztondo, N., Liao, D., Boisvert, W.A., Evans, R.M., and Curtiss, L.K. (2003). Transcriptional repression of atherogenic inflammation: modulation by PPARdelta. Science *302*, 453–457. https://doi.org/10.1126/science.1087344.

62. Sindhu, S.T.A.K., Ahmad, R., Blagdon, M., Ahmad, A., Toma, E., Morisset, R., and Menezes, J. (2003). Virus load correlates inversely with the expression of cytotoxic T lymphocyte activation markers in HIV-1-infected/AIDS patients showing MHC-unrestricted CTL-mediated lysis. Clin. Exp. Immunol. *132*, 120–127. https://doi.org/10.1046/j.1365-2249.2003.02120.x.

63. Sindhu, S., Akhter, N., Kochumon, S., Thomas, R., Wilson, A., Shenouda, S., Tuomilehto, J., and Ahmad, R. (2018). Increased Expression of the Innate Immune Receptor TLR10 in Obesity and Type-2 Diabetes: Association with ROS-Mediated Oxidative Stress. Cell. Physiol. Biochem. *45*, 572–590. https://doi.org/10.1159/000487034.

STAR★METHODS

KEY RESOURCES TABLE

REAGENT or RESOURCE	SOURCE	IDENTIFIER
Antibodies		
PE Mouse Anti-Human CD11c	BD Biosciences	347637
PE/Cyanine7 anti-mouse CD11c	BioLegend	117317
APC Mouse Anti-Human CD11b (D12)	BD Biosciences	340936
Alexa Fluor® 488 Mouse Anti-Human CD11b	BD Pharmingen	557701
FITC anti-human HLA-DR Antibody	Beckman coulter	IM1639U
FITC Mouse anti Human CD80	Bio-Rad	MCA2071F
PE anti-human CD192 (CCR2) Antibody	BioLegend	357206
PE Mouse Anti-Human CD163	BD Pharmingen	556018
APC Mouse Anti-Mouse CD36	BD Pharmingen	562744
FITC Mouse Anti-CD36 Monoclonal Antibody (MF3)	Invitrogen	MA5-16832
APC Anti-mouse - CD11c Antibody	Miltenyi Biotec	130-110-702
V450 Rat Anti-Mouse CD45	BD Horizon	560501
PE Mouse CX3CL1/Fractalkine Antibody	r&d systems	FAB571P
FITC Anti-mouse-Ly-6C Antibody	Miltenyi Biotec	130-111-777
PE-Cy™7 Mouse Anti-Human CD11b	BD Biosciences	2044736
PE Mouse Anti-Human CD126	BD Biosciences	551850
Alexa Fluor® 647 Rat Anti-Mouse CD124	BD Biosciences	564084
PE Mouse Anti-Human IL-1β	BD Biosciences	340516
Anti-FABP4 antibody [9B8D]	Abcam	ab93945
PE Mouse anti-JNK (pT183/pY185)	BD Biosciences	562480
Pacific Blue Mouse anti-p38 MAPK (pT180/pY182)	BD Bioscience	560313
PE-Cy™7 Mouse anti-p38 MAPK (pT180/pY182)	BD Bioscience	560241
Alexa Fluor® 488 Mouse Anti-ERK1/2 (pT202/pY204)	BD Bioscience	612592
PE Mouse anti-NF-κB p65 (pS529)	BD Bioscience	558423
Alexa Fluor® 647 Mouse anti-IκBα	BD Phosflow	560817
Alexa Fluor®488 Mouse IgG2a, κ Isotype control	BD Phosflow™	558055
PE Mouse IgG2b, κ Isotype Control	BD Pharmingen™	559529
PE-Cy™7 Mouse IgG2b, κ Isotype Control	BD Pharmingen™	560542
CD36 (D8L9T) Rabbit mAb	Cell signaling	14347
CD11c (D3V1E) XP ® Rabbit mAb	Cell signaling	45581
FABP5 (D1A7T) Rabbit mAb	Cell signaling	39926S
FABP4 (D25B3) XP ® Rabbit mAb	Cell signaling	3544S
Anti-PPAR delta antibody	Abcam	ab8937
Perilipin-2/ADFP Antibody - BSA Free	NOVUS	NB110-40878
Phospho-p44/42 MAPK (Erk1/2) (Thr202/Tyr204) (D13.14.4E) XP® Rabbit mAb	Cell signaling	4370S
p44/42 MAPK (Erk1/2) (137F5) Rabbit mAb	Cell signaling	4695
NF-κB p65 (D14E12) XP ® Rabbit mAb	Cell signaling	8242S
Phospho-NF-κB p65 (Ser536) (E1Z1T) Mouse mAb	Cell signaling	13346s
Phospho-p38 MAPK (Thr180/Tyr182) Antibody	Cell signaling	9212S

(*Continued on next page*)

Continued

REAGENT or RESOURCE	SOURCE	IDENTIFIER
Phospho-p38 MAPK (Thr180/Tyr182) (28B10) Mouse mAb	Cell signaling	9216L
SAPK/JNK Antibody	Cell signaling	9252S
Phospho-SAPK/JNK (Thr183/Tyr185) Antibody	Cell signaling	9251S
β-Actin Antibody	Cell signaling	4967S
Biological samples		
Human Peripheral Blood Mononuclear Cell (PBMC)	Dasman Diabetes Institute	N/A
Mice Peripheral Blood Mononuclear Cell (PBMC)	Dasman Diabetes Institute	N/A
Chemicals, peptides, and recombinant proteins		
Phorbol-12-myristate-13-acetate (PMA)	Sigma-Aldrich	79346-5MG
Triacsin C from Streptomyces sp.	Sigma-Aldrich	T4540-1MG
2-Fluoropalmitic acid	Santa Cruz Biotechnology	SC-202881A
GW0742 inhibitor	Sigma-Aldrich	G3295-1MG
Rosiglitazone	Sigma-Aldrich	R2408-10MG
Bovine serum albumin	Sigma-Aldrich	A3294-50G
Sodium palmitic acid	Sigma-Aldrich	P9767-5G
Critical commercial assays		
RNeasy Mini Kit	QIAGEN	74104
High-capacity cDNA reverse transcription kit	Applied Biosystems	43-688-14
TaqMan® Gene Expression Master Mix	Applied Biosystems	A15298
VIROMER BLUE for siRNA ttansfection	Lipocalyx	VB-01LB-00
Acyl-CoA synthetase activity assay kit	BioVision's	K184-100
Experimental models: Cell lines		
Human monocytic THP-1 cells	ATCC	TIB-202
Experimental models: Organisms/strains		
Mouse: Male C57BL/6	Jackson Laboratories	RRID:IMSR_JAX:000664
Oligonucleotides		
ACSL1 Silencer ® select validated siRNA	ThermoFisher(Ambion)	4390824, ID: s4996
Primers for: ACSL1	ThermoFisher	Hs00960561_m1
Primers for: ACSL3	ThermoFisher	Hs00244853_m1
Primers for: ACSL4	ThermoFisher	Hs00244871_m1
Primers for: ACSL5	ThermoFisher	Hs01061754_m1
Primers for: ACSL6	ThermoFisher	Hs00922295_m1
Primers for: CD36	ThermoFisher	Hs00354519_m1
Primers for: FABP4	ThermoFisher	Hs01086177_m1
Primers for: FABP5	ThermoFisher	Hs02339439_g1
Primers for: CPT-1A	ThermoFisher	Hs00912671_m1
Primers for: CPT-1B	ThermoFisher	Hs00189258_m1
Primers for: CPT-2	ThermoFisher	Hs00988962_m1
Primers for: ACACA	ThermoFisher	Hs01046047_m1
Primers for: ITGAX (CD11C)	ThermoFisher	Hs00174217_m1
Primers for: TNF-A	ThermoFisher	Hs01113624_g1
Primers for: IL-1B	ThermoFisher	Hs01555410_m1
Primers for: IL-10	ThermoFisher	Hs00961622_m1
Primers for: PPAR GAMMA	ThermoFisher r	Hs01115513_m1

(*Continued on next page*)

Continued

REAGENT or RESOURCE	SOURCE	IDENTIFIER
Primers for: PPAR DELTA	ThermoFisher	Hs04187066_g1
Primers for: PPAR ALPHA	ThermoFisher	Hs00231882_m1
Primers for: GAPDH	ThermoFisher	Hs03929097_g1
Software and algorithms		
FACSDivaTM Software 8	BD Biosciences	https://www.bdbiosciences.com/en-eu/products/software/instrument-software/bd-facsdiva-software
Zeiss Zen 2010 control software	Zeiss	https://www.zeiss.com/microscopy/en/products/software/zeiss-zen.html
GraphPad Prism software	Graph Pad Software	https://www.graphpad.com/features
Other		
BioRender	BioRender	https://www.biorender.com/

RESOURCE AVAILABILITY

Lead contact

Further information and requests for resources and reagents should be directed to and will be fulfilled by the lead contact, Rasheed Ahmad (rasheed.ahmad@dasmaninstitute.org).

Materials availability

This study did not generate new unique reagents.

Data and code availability

- Data reported in this paper will be shared by the lead contact upon request.
- This paper does not report any original code.
- Any additional information required for data reported in this paper is available from the lead contact upon reasonable request.

EXPERIMENTAL MODEL AND SUBJECT DETAILS

Cell culture

Human monocytic THP-1 cells were purchased from American Type Culture Collection (ATCC) and grown in RPMI-1640 culture medium (Gibco, Life Technologies, Grand Island, USA) supplemented with 10% fetal bovine serum (Gibco, Life Technologies, Grand Island, NY, USA), 2 mM glutamine (Gibco, Invitrogen, Grand Island, NY, USA), 1 mM sodium pyruvate, 10 mM HEPES, 100 ug/ml Normocin, 50 U/ml penicillin and 50 μg/ml streptomycin (P/S; (Gibco, Invitrogen, Grand Island, NY, USA). They were incubated at 37°C (with humidity) in 5% CO_2. TLR4-/- THP1 cells were purchased from InvivoGen (San Diego, CA, USA) and cultured in a complete RPMI medium containing Blasticidin and Zeocin antibiotics. THP1-defMyD (MyD88-/-) cells were purchased from InvivoGen (San Diego, CA, USA) and cultured in a complete RPMI medium containing Zeocin (200 μg/ml) and HygroGold (100 μg/ml). THP1 with control plasmid was purchased from InvivoGen (San Diego, CA, USA) and cultured in a complete RPMI medium containing Zeocin (200 μg/ml). Before stimulation, THP-1 cells were transferred into a normal medium.

Isolation of human peripheral blood mononuclear cells (PBMC) and monocyte purification

Human peripheral blood samples (20-30 ml each) from healthy volunteers following informed consent were collected in EDTA vacutainer tubes and processed for PBMC isolation using the Ficoll-Hypaque density gradient method as described elsewhere.[62,63] Briefly, primary monocytes were isolated from PBMC by negative selection, following the manufacturer's instructions (Human monocyte isolation kit II, MACS Miltenyi Biotec GmbH, Germany). PBMC (~10^7 cells) were resuspended in 30μl PBS (containing 0.5% BSA and 2 mM EDTA; pH 7.2) and 10 μl FcR blocking reagent. After gentle mixing, a 10 μl biotin-labeled antibody cocktail (antibodies reacting with CD3, CD7, CD16, CD19, CD56, CD123, and glycophorin-A human antigens) was added to conjugate and remove T and B lymphocytes, dendritic cells, NK cells, and basophils.

After incubation for 10 min on wet ice, 30 μl sample buffer and 20 μl anti-biotin antibodies labeled microbeads were added, mixed, and again incubated on wet ice for 15 min. After washing, the pellet was resuspended in 500 μl suspension buffer and passed through the MACS separator column, and effluent containing the enriched monocyte fraction was collected and purity for $CD14^+$ cells was assessed by flow cytometry, which was found to be >90% for each monocyte fraction isolated.

Mice studies

Male C57BL/6 mice were purchased from Jackson Laboratories. Animal studies were approved by the Dasman Diabetes Institute Institutional Animal Care Committee. Mice were fed a standard chow diet (8664; Harlan Teklad; 6.4% w/w fat) and maintained under a regular 12/12-h light/dark cycle at a room temperature of 23°C. To test the effect of triacsin C, 8 to 9-week-old male mice were fasted overnight and then given triacsin C (10mg/kg) or vehicle by oral gavage. After 30 min of the resting period, mice were given 30g of high-fat diet (HFD) (58% Kcal from fat; #D12331I, Research Diets, Inc.). Tail vein blood samples (50-60 μl each) were collected from each mouse before and four hours after drug administration.

METHOD DETAILS

Cell stimulation

Monocytic cells were plated in 12-well plates (Costar, Corning Incorporated, Corning, NY, USA) at 1×10^6 cells/well concentration unless indicated otherwise. Before stimulation, monocytic cells were differentiated into macrophages with 10ng/ml phorbol-12-myristate-13-acetate (PMA) for three days, followed by three days rest in serum-PMA-free RPMI media before they were considered ready for treatment. To induce short-term PA stimulation mimicking the effect of AHFF, differentiated macrophages were stimulated with PA (150μM conjugated with bovine serum albumin (BSA), see below) or 0.1% BSA as a control (vehicle) for 4h at 37°C. Cells were harvested for either total RNA or protein isolation, and the culture media were collected for measuring cytokines secretion. For various stimulation studies, differentiated macrophages were pre-treated with ACSL1 inhibitor, triacsin C (5 μM; T4540), 2-Fluoro Palmitic acid (0.2mM/ml), peroxisome proliferator-activated receptor (PPAR)-δ agonist GW0742 (1μM), or PPARγ agonist rosiglitazone (1μM) for 30–60 min, then stimulated with PA (150 μM) or with vehicle (0.1% BSA) for 4h at 37°C.

Preparation of palmitic acid

Bovine serum albumin (10.5%) was dissolved in 25 mM HEPES/DMEM, and syringe filtered (0.22 μM, Millipore). Sodium palmitic acid (100 mM) was heated until dissolved in endotoxin-free water and rapidly added to warmed BSA solution (6:1 molar ratio). Then, this BSA-conjugated PA was added to reach the indicated concentration of PA.

Real-time quantitative RT-PCR

Total RNA was extracted using RNeasy Mini Kit (Qiagen, Valencia. CA, USA) as per the manufacturer's instructions. cDNA was synthesized using 1μg of total RNA using a high-capacity cDNA reverse transcription kit (Applied Biosystems, Foster City, CA, USA). Real-time PCR was performed on 7500 Fast Real-Time PCR Systems (Applied Biosystems, Foster City, CA, USA) using TaqMan® Gene Expression Master Mix (Applied Biosystems, Foster city). Each reaction contained 50ng cDNA that was amplified with Inventoried TaqMan Gene Expression Assay products (key resources table). The threshold cycle (Ct) values were normalized to the housekeeping gene GAPDH, and the amounts of target mRNA relative to control were calculated with ΔΔCt-method.[16,45] Relative mRNA expression was expressed as fold expression over an average of control gene expression. The expression level in the control treatment was set at 1. Values are presented as mean ± SEM. $P< 0.05$ was considered significant.

Flow cytometry analysis

Cultured macrophages were centrifugated at 300g for 5 min, the supernatant was discarded, and cells were resuspended in FACS staining buffer (BD Biosciences) and blocked with human IgG (Sigma; 20 μg) for 30 min on ice. Cells were washed and resuspended in 100 μl of FACS buffer and incubated with specific macrophage markers (key resources table) on ice for 30 min. Cells were washed three times with FACS buffer and resuspended in 2% paraformaldehyde (PFA). Cells were centrifuged and resuspended in FACS buffer for FACS analysis (FACSCanto II; BD Bioscience, San Jose, USA). FACS data analysis was performed using BD FACSDiva™ Software 8 (BD Biosciences, San Jose, USA). Unstained cells were used to set the quadrant of the negative vs positive gates. For intracellular staining, cells were incubated

with fixation/permeabilization buffer (Cat# 00-5523-00, eBioscience, San Diego, CA, USA) for 20 min in 4°C, followed by washing and staining with an intracellular inflammatory marker (key resources table) or signaling protein for 30 min. The cells were then washed and resuspended in PBS supplemented with 2% FCS for FACS analysis (FACSCanto II; BD Bioscience, San Jose, USA). FACS data analysis was performed using BD FACSDivaTM Software 8 (BD Biosciences, San Jose, USA). Gating strategies are summarized in Figure S5.

Cytokine secretion

Transformed macrophage cells were stimulated with PA in the presence and absence of triacsin C. Secreted IL-1β, TNF-α, and MCP-1 were quantified in the collected supernatants using sandwich ELISA following the manufacturer's instructions (R&D systems, Minneapolis, USA).

Small interfering RNA (siRNA) transfections

Differentiated macrophages were transfected with 20 nM of the siRNA using Viromer Blue (Lipocalyx, Halle, Germany) according to the manufacturer's instructions. ACSL1 gene knockdown level was assessed by real-time-qPCR and western blotting.

Measurement of Acyl-CoA synthetase activity

Acyl-CoA synthetase activity was determined through the use of an Acyl-CoA synthetase activity assay kit (Cat #. K184-100, BioVision's, Milpitas, California) according to the manufacturer's protocol. In brief, THP-1 cells were cultured and differentiated as mentioned before. 50 mg of cells were homogenized in a buffer containing 20 mM HEPES, 1 mM EDTA, and 250 mM sucrose, pH 7.4. After centrifugation at 10,000 ×g, cell lysates were collected, and the protein concentration of cell lysates was determined Bradford assay before the ACS activity assay.

Samples, 5 μl each, were loaded in wells in a 96-well plate in duplicate (Sample and Sample background), and the final volume was adjusted to 50 μl with ACS assay buffer. For positive control, 2 μl of the provided positive control was used with sample adjustment to 50 μl total volume with ACS buffer. H_2O_2 standard curve was created in duplicates similarly. The reaction was initiated by adding 50 μl of reaction mix into Standard and samples wells and 50 μl of background control mix (with no ACS substrate) into the sample background. The reaction was measured at Ex/Em= 535/587 in kinetic mode for 30 min at 37°C. The maximum signal was reached in 8 min and two points in the liner range of the reaction were chosen as t1 and t2. Background readings were subtracted from all sample readings. H_2O_2 amount from the standard curve was determined during the reaction time (Δt= t2-t1) in nmol (B) through the use of the following formula: ΔRFU= RFU1 -RFU2 and the sample Acyl-CoA synthetase activity was calculated using the following formula: $B/(\Delta t \times V) \times D$ = nmol/min/ml = mU/ml

Confocal microscopy

To detect lipid accumulation by confocal microscopy, macrophages seeded on coverslips were fixed with 4% PFA for 20 min, washed two times with PBS, and then stained with Nile Red (Segma-Aldrich, Cat; 72485). Cells were washed three times in PBS then counterstained and mounted over slides using mounting media containing DAPI (Vectashield, Vectorlab, H1500).

For ACSL1 and FABP4 double staining, cells were cultured and treated on coverslips as mentioned above. Cells were then fixed with 4% PFA for 20 min followed by 10 min incubation in permeabilization buffer (PBS containing 0.5% saponin). Cells were washed three times for five min followed by blocking in PBS that contain 0.1% Tween 20 and 1% BSA for 30 min. Cells were incubated overnight at 4°C with primary antibodies for anti-ACSL1 rabbit (Cell signaling; 9189S) and anti-FABP4 mouse antibodies (Abcam; ab93945). Cells were washed again followed by incubation in a secondary antibody appropriate for each specie. Cells were washed three times, 5 min each, in PBS, counterstained, and then mounted over slides using mounting media containing DAPI (Vectashield, Vectorlab, H1500).

Confocal images were obtained by using an inverted Zeiss LSM710 spectral confocal microscope (Carl Zeiss, Gottingen, Germany) and EC Plan-Neofluar 40×/1.30 oil DIC M27 objective lens. After exciting samples with a 543 nm HeNe laser and 405 nm line of an argon ion laser, optimized emission detection bandwidths were configured by using Zeiss Zen 2010 control software. All samples were analyzed using

the same parameters and the resulting color markup of analysis was confirmed for each sample. The Correlated Total Cell Fluorescence (CTCF) was calculated by using the following equation: CTCF=IntDen−(Area of selected cells X background mean grey value (BMGV)).

Western blotting

Differentiated macrophages were harvested and incubated for 30 min with lysis buffer (Tris 62.5 mM (pH 7.5), 1% Triton X-100, 10% glycerol). The lysates were then centrifuged at 14000 ×g for 10 min and the supernatants were collected. Protein concentration in lysates was measured by Quickstart Bradford Dye Reagent, 1x Protein Assay kit (Bio-Rad Laboratories, Inc, CA). Protein (20 μg) samples were mixed with sample loading buffer, heated for 5 min at 95°C, and resolved by 12% SDS-PAGE. Cellular proteins were transferred to the Immuno-Blot PVDF membrane (Bio-Rad Laboratories, USA) by electroblotting. The membranes were then blocked with 5% non-fat milk in PBS for 1h, followed by incubation with primary vvantibodies purchased from Cell Signaling Technology, Inc; please see key resources table for more details. The blots were then washed four times with TBS and incubated for 2h with HRP-conjugated secondary antibody (Promega, Madison, WI, USA). Immunoreactive bands were developed using an Amersham ECL plus Western Blotting Detection System (GE Health Care, Buckinghamshire, UK) and visualized by Molecular Imager ® ChemiDoc^{TM}MP Imaging Systems (Bio-Rad Laboratories, Hercules, CA, USA).

Ethics

Written informed consent was obtained from all study participants (healthy volunteers) in accordance with the ethical guidelines of the Declaration of Helsinki and study approval by the Kuwait Ministry of Health Ethical Board (Approval ID#: 1806/2021) and Ethical Review Committee (ERC) of Dasman Diabetes Institute, Kuwait (Approval ID#: RA MoH-2022-002).

All mice used in these experiments were bred and handled in accordance with animal studies that were approved by the Dasman Diabetes Institute Institutional Animal Care Committee (RA AM-2016-007).

QUANTIFICATION AND STATISTICAL ANALYSIS

Statistical analysis was performed using GraphPad Prism software (La Jolla, CA, USA). Data are shown as mean ± standard error of the mean unless otherwise indicated. Unpaired Student t-test and one-way ANOVA with Tukey' test were used to compare means between groups. For all analyses, data from a minimum of three sample sets were used for statistical calculation. P value <0.05 was considered significant. ns: non-significant, *P < 0.05, **P<0.01, ***P< 0.001 and ****P < 0.0001, compared to respective control.